Article

Colorless Polyimides Derived from Octahydro-2,3,6,7-anthracenetetracarboxylic Dianhydride

Masatoshi Hasegawa *[iD]**, Hiroki Sato, Katsuhisa Hoshino, Yasuhisa Arao and Junichi Ishii**

Department of Chemistry, Faculty of Science, Toho University, 2-2-1 Miyama, Funabashi 274-8510, Chiba, Japan
* Correspondence: mhasegaw@chem.sci.toho-u.ac.jp

Abstract: A cycloaliphatic tetracarboxylic dianhydride, octahydro-2,3,6,7-anthracenetetracarboxylic dianhydride (OHADA) was synthesized to obtain novel colorless polyimides (PIs). Herein, approaches for decolorizing an OHADA prototype and simplifying the entire process are described, and a plausible steric structure for OHADA is proposed. The polyaddition of OHADA and 2,2′-bis(trifluoromethyl)benzidine (TFMB) was unsuccessful; specifically, the reaction mixture remained inhomogeneous even after prolonged stirring. However, the modified one-pot process was applicable to the OHADA/TFMB system. The isolated PI powder form, as well as those for the other OHADA-based PIs, was highly soluble in numerous solvents and afforded a homogeneous and stable solution with a high solid content (20–30 wt%). Solution casting produced a colorless and ductile PI film with a very high glass transition temperature (T_g~300 °C). Furthermore, the OHADA/TFMB system exhibited remarkable thermal stability compared with those of the other related TFMB-derived semi-cycloaliphatic PIs. However, contrary to our expectations, this PI film did not exhibit a low linear coefficient of thermal expansion (CTE). This PI film also possessed excellent thermoplasticity, probably reflecting its peculiar steric structure. The use of an amide-containing diamine significantly enhanced the T_g (355 °C) and somewhat reduced the CTE (41.5 ppm K^{-1}) while maintaining high optical transparency and excellent solubility.

Keywords: colorless polyimides; cycloaliphatic (alicyclic) tetracarboxylic dianhydride; octahydro-2,3,6,7-anthracenetetracarboxylic dianhydride; optical transparency; heat resistance; linear coefficient of thermal expansion (CTE); tensile properties; solubility; thermoplasticity

1. Introduction

The significance of optically transparent, heat-resistant polymeric materials has been increasingly recognized in recent years owing to their potential applications as optoelectronic materials, including plastic substrates as alternatives to current non-alkali glass substrates, dielectric films of optically transparent flexible printed circuits, and cover window layers in organic light-emitting diode display devices. Colorless poly(ether sulfone) (PES) is one of super engineering plastics with the highest class of heat resistance (T_g = 225 °C) [1]. However, the heat resistance of PES is not always sufficient for optoelectronic applications.

Wholly aromatic polyimides (PIs) have been used as dielectric materials in various electronic devices owing to their extremely high heat resistance and reliable electrical insulation ability. Therefore, the chemistry, physics, properties, structures, characterization, and applications of PIs have been extensively studied [2–18]. However, conventional wholly aromatic PI films are typically intensely colored owing to intra- and intermolecular charge-transfer (CT) interactions [19], which often hinder their optoelectronic applications. Wholly aromatic PIs without coloration are substantially limited to the PI derived from 4,4′-(hexafluoroisopropylidene)diphthalic anhydride (6FDA) and 2,2′-bis(trifluoromethyl)benzidine (TFMB) [20,21]. Colorless PIs have been extensively investigated in industry and academia from their practical values.

The use of aliphatic monomers [usually, cycloaliphatic (alicyclic) for ensuring sufficient heat resistance], either in diamines, tetracarboxylic dianhydrides, or both, effectively decolorizes PI films [19,22–50]. However, when cycloaliphatic diamines were used, insoluble salts are formed between the free aliphatic amino groups and the COOH groups of the low-molecular-weight amic acids yielded in the initial reaction stage, disturbing the smooth progress of the reaction [39]. By contrast, the use of cycloaliphatic tetracarboxylic dianhydrides in combination with aromatic diamines inhibits salt formation, allowing the polyaddition to proceed smoothly. This type of semi-cycloaliphatic PIs has therefore been studied extensively [27–46].

Despite their advantages, mass-produced cycloaliphatic tetracarboxylic dianhydrides are not always abundantly available. Figure 1 shows the reduced viscosities (η_{red}) of several related PI precursors, poly(amic acid)s (PAAs), which can provide an approximate indication of polyaddition reactivity (polymerizability). The polymerizability of bicyclo[2.2.2]oct-7-ene-2,3,5,6-tetracarboxylic dianhydride (BTA) with TFMB was insufficient, as illustrated by its very low η_{red} value (0.12 dL g^{-1}), corresponding to the absence of film-forming ability of the resultant PAA. 1S,2R,4S,5R-Cyclohexanetetracarboxylic dianhydride (H-PMDA) showed slightly higher polymerizability with TFMB (η_{red} = 0.38 dL g^{-1}) than BTA. However, the resultant PAA exhibited poor film-forming ability, as indicated by cracks generated in the cast film. By contrast, 1,2,3,4-cyclobutanetetracarboxylic dianhydride (CBDA) exhibited considerably higher polymerizability with TFMB (Figure 1), allowing for the formation of a ductile thermally imidized film [32,51]. The high polymerizability of CBDA is explained by the ring strain of the acid anhydride functional groups [32].
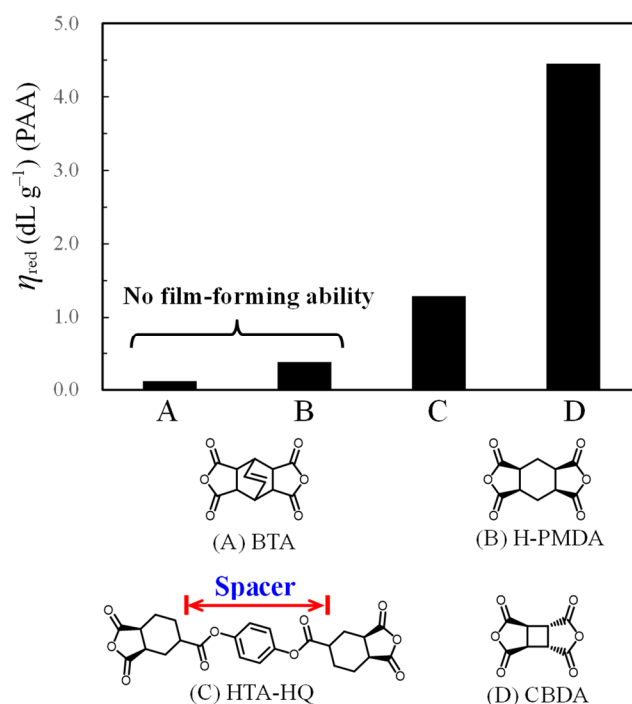

Figure 1. The η_{red}-based relative polymerizability of typical mass-produced cycloaliphatic tetracarboxylic dianhydrides (BTA, H-PMDA, and CBDA) with TFMB. Equimolar polyaddition was conducted in DMAc for 72 h at an initial monomer content of 30 wt% with gradual dilution for ensuring effective magnetic stirring. CBDA was sublimated just before use for the acid anhydride ring closure of a partially hydrolyzed portion.

However, the manufacturing process of CBDA is expensive owing to the required UV-irradiation process [27,32], which hinders its large-scale production. In addition, CBDA-based PIs often exhibit poor solution-processability [32]. A new, highly reactive cy-

cloaliphatic tetracarboxylic dianhydride that can be manufactured on a large scale without UV irradiation is expected to provide novel solution-processable colorless PIs.

The relatively low polymerizability of H-PMDA can be explained by the steric hindrance related to the adjacent bis-*exo* functional groups [31]. To reduce this steric hindrance, we designed previously a cycloaliphatic tetracarboxylic dianhydride (HTA-HQ [30]), which included a *para*-phenylene spacer inserted via ester linkages between the functional groups. As expected, HTA-HQ exhibited significantly enhanced polymerizability with TFMB (Figure 1). However, the rotatable single bonds in the HTA-HQ structure can contribute to a reduction in the T_g [30].

Therefore, we focused on a novel cycloaliphatic tetracarboxylic dianhydride with a ladder-like spacer without rotatable single bonds, octahydro-2,3,6,7-anthracenetetracarboxylic dianhydride (OHADA) [52]. This new monomer is expected to significantly improve the polymerizability owing to its spacer effect while further enhancing the T_g of the resultant PI films owing to its rigid ladder-like structure. The present study was inspired by previous work, in which the synthesis of 9,10-diphenoxy- or 9,10-dialkoxy-substituted OHADA analogs and some limited properties of the resultant PIs (solubility and thermal stability) were reported [53–55]. However, it remained unclear whether these materials are valuable for optoelectronic applications since other important properties (optical transparency, glass transition temperatures, thermal expansion property, mechanical properties, and thermoplasticity) were not provided in the previous studies. In addition, no studies on PIs using non-substituted OHADA have so far been conducted, even though this non-substituted monomer is expected to afford PIs with higher performance (e.g., heat resistance) than that of the counterparts from the 9,10-disubstitited ones owing to the prevention of dense chain stacking by these side groups. The present study describes the synthesis and thorough decolorization process of non-substituted OHADA, its polymerizability with aromatic diamines, and the detailed properties of the OHADA-based PI films. The PIs derived from the decolorized non-substituted OHADA afforded novel high-temperature materials suitable for optoelectronic applications.

2. Experimental Section

2.1. Materials

2.1.1. Synthesis of OHADA Prototype

OHADA was synthesized according to the reaction scheme (Figure 2) involving tetrabromination of the methyl groups of durene to obtain 1,2,4,5-tetrakis(bromomethyl)benzene (TBrMB) and subsequent Diels-Alder reaction of TBrMB and maleic anhydride (MAn) in the presence of NaI [53,54]. It is believed that the Diels-Alder reaction occurs via an active intermediate, 1,2,4,5-tetrakis(iodomethyl)benzene generated by halogen exchange. The detailed synthetic procedures are described below.
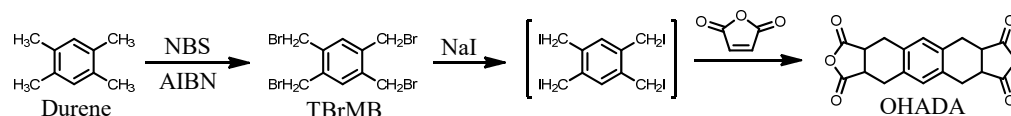

Figure 2. Reaction scheme for the synthesis of OHADA.

TBrMB. In a 300 mL-three-necked flask, durene (50 mmol, 6.83 g) and *N*-bromosuccinimide (NBS, 250 mmol, 44.69 g) were dissolved in CCl$_4$ (110 mL) in the presence of azobis (isobutyronitrile) (AIBN, 0.70 g). The solution was refluxed at 60 °C for 1 h in an N$_2$ atmosphere with vigorous stirring. The completion of the reaction was confirmed by thin layer chromatography (TLC). An undissolved portion (mainly, NBS residue) was filtered out, and the filtrate was concentrated using an evaporator. The precipitate formed was collected by filtration and washed with cold ethanol (yield: 50%). The crude product was recrystallized from a mixed solvent (ethyl acetate/ethanol, 1/1, *v/v*) and dried at 60 °C for 12 h under vacuum. The analytical data for the product are as follows. Melting point

[differential scanning calorimetry (DSC)]: 156 °C. FT-IR (KBr plate method, cm^{-1}): 3021 (C$_{arom}$–H stretching), 2975 (CH$_2$, C$_{aliph}$–H), 603 (C–Br). ^{1}H-NMR (400 MHz, CDCl$_3$, δ, ppm): 7.38 [s, 2H (relative integrated intensity: 2.00H), Ar–H], 4.60 [s, 8H (8.06H), CH$_2$Br]. The ^{1}H-NMR data of the starting material (durene) are also shown for comparison: 6.91 [s, 2H (2.00H), Ar–H], 2.20 [s, 12H (12.01H), CH$_3$]. These results confirmed that the product is the desired tetrabromide (TBrMB).

The tetra-bromination was sensitive to the reaction temperature and time; when the bromination reaction was conducted at 60 °C for 2 h or longer, the proton signals at δ = 7.38 and 4.60 ppm of TBrMB changed from singlet to multiplet, suggesting the formation of some impurities including further brominated CHBr$_2$ groups. Therefore, the reaction was conducted at 60 °C for 1 h as the optimal conditions for obtaining pure TBrMB.

OHADA. In a 100 mL-three-necked flask, TBrMB (10 mmol, 4.52 g) and MAn (30 mmol, 3.01 g) were dissolved in *N,N*-dimethylformamide (DMF, 30 mL) in the presence of NaI (100 mmol, 15.11 g). The reaction mixture was refluxed at 150 or 160 °C for 9 h with continuous vigorous stirring. The progress of the reaction was monitored by TLC. The reaction mixture was gradually poured into a large quantity of water, and the precipitate formed was collected by filtration and dried at 250 °C for 12 h under vacuum. Black-brown product was obtained (yield: 60%). The analytical data for the product are as follows. Melting point (DSC): 405 °C (single peak). FT-IR (KBr plate method, cm^{-1}): 3031 (C$_{arom}$–H stretching), 2972 (CH$_2$, C$_{aliph}$–H), 1840/1773 (acid anhydride, C=O). ^{1}H-NMR (400 MHz, dimethyl sulfoxide (DMSO)-d_6, δ, ppm): 7.05 [s, 2H (2.00H), Ar–H], 3.72 [s (br), 4H (4.05H), CH–C=O], 2.97–2.85 [m, 8H (8.01H), Ar–CH$_2$]. Elemental analysis, Anal. Calcd (%) for C$_{18}$H$_{14}$O$_6$ (326.31): C, 66.26; H, 4.32. Found: C, 65.87; H, 4.21. The results confirmed that the product is the desired compound (OHADA).

2.1.2. Synthesis of Amide-Type Diamine

An amide-type diamine (AB-TFMB) was synthesized according to the reaction scheme (Figure 3), as described in our previous studies [44,45]. The analytical data for the product are as follows. Melting point (DSC): 317 °C. FT-IR (KBr plate method, cm^{-1}): 3418 (amine N–H stretching), 3303 (amine + amide N–H), 3096/3039 (C$_{arom}$–H), 1655 (amide, C=O), 1509 (1,4-phenylene), 1311 (C–F). ^{1}H-NMR (400 MHz, DMSO-d_6, δ, ppm): 10.16 [s, 2H (2.00H), NHCO], 8.33 [sd, 2H (2.02H), *J* = 1.7 Hz, 3,3′-protons of the central biphenylene unit (BP)], 8.07 [dd, 2H (1.97H), *J* = 8.4, 1.6 Hz, 5,5′-protons of BP], 7.77 [d, 4H (4.05H), *J* = 8.6 Hz, 3,3′,5,5′-protons of the terminal aniline unit (AN)], 7.32 [d, 2H (2.03H), *J* = 8.4 Hz, 6,6′-protons of BP], 6.64 [d, 4H (4.02H), *J* = 8.5 Hz, 2,2′,6,6′-protons of AN], 5.86 [s, 4H (3.99H), NH$_2$]. Elemental analysis, Anal. Calcd (%) for C$_{28}$H$_{20}$O$_2$N$_4$F$_6$ (558.47): C, 60.22; H, 3.61; N, 10.03. Found: C, 60.00; H, 3.87; N, 9.98. The results confirmed that the product is the desired diamine (AB-TFMB).
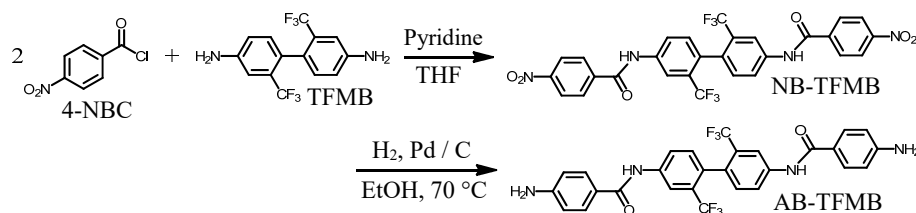

Figure 3. Reaction scheme for the synthesis of amide-type diamine (AB-TFMB).

2.1.3. Common Monomers

Common monomers [4,4′-oxydianiline (4,4′-ODA), TFMB, and CBDA] were used in this study. The commercial sources and melting points of the common monomers and raw materials used are listed in Supplementary Materials Tables S1 and S2.

2.1.4. Polymerization, Imidization, and PI Film Preparation

Polymerization, imidization, and film preparation were conducted via three different routes (Figure 4): conventional two-step process (Route T), chemical imidization process (Route C), and a modified one-pot process (Route R).
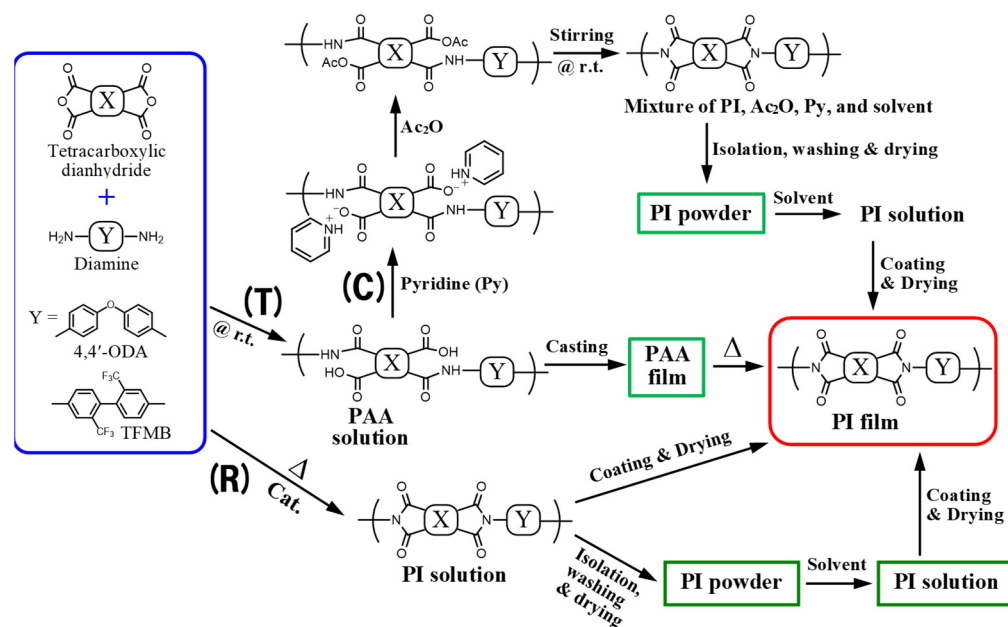

Figure 4. Schemes of polymerization, imidization, and film preparation processes via different routes: (T) two-step process, (C) chemical imidization process in solution, and (R) one-pot process by refluxing the reaction mixtures in the presence of catalysts.

The two-step process (T) includes polyaddition, solution casting of the resultant PAAs, and thermal imidization of the PAA cast films. Polyaddition was conducted by adding tetracarboxylic dianhydride powder (1 mmol) to the *N*-methyl-2-pyrrolidone (NMP) solution of diamine (1 mmol) with an initial total solid content of 30 wt% in a sealed bottle with continuous magnetic stirring at room temperature for 72 h. During the polyaddition, the reaction mixture was gradually diluted as appropriate with a minimum quantity of the same solvent to ensure effective magnetic stirring. The resultant PAA solution was diluted as appropriate, bar-coated on a glass substrate, and dried at 80 °C for 2 h in an air-convection oven. The PAA film obtained was thermally imidized at 200 °C for 1 h + 300 °C for 1 h on the substrate under vacuum, and subsequently, annealed at 300 °C for 1 h under vacuum without the substrate to remove residual stress.

The chemical imidization process (C) includes chemical imidization of the PAAs in solution, isolation of PI powder, redissolution of the PI powder in a fresh solvent, and the formation of PI films by solution casing. Chemical imidization was conducted by gradually adding a cyclodehydration agent [acetic anhydride (Ac_2O)/pyridine (7/3, *v/v*)] to the PAA solutions at a fixed molar ratio of $[Ac_2O]/[COOH]_{PAA} = 5$ with continuous stirring at room temperature for 12 h in a sealed bottle. This process is applicable only to highly soluble PI systems, otherwise gelation or precipitation, which prevents the subsequent casting process, occurs during the reaction. The resultant homogeneous reaction mixture was diluted as appropriate with the same solvents and gradually poured into a large quantity of poor solvents (methanol or water). The fibrous white precipitate formed was collected by filtration, dried at 100 °C for 12 h under vacuum, and redissolved in fresh anhydrous γ-butyrolactone (GBL) at a high solid content (20–30 wt%). The PI films were prepared as follows, unless otherwise specified. The obtained homogeneous PI solution was coated on a glass substrate and dried at 80 °C for 2 h in an air convection oven, and subsequently, heated at 150 °C for 0.5 h + 200 °C for 0.5 h + 250 °C for 1 h under vacuum on the substrate.

The PI films (typically, 20 μm thick) were then annealed at 250 °C for 1 h without the substrate to remove residual stress.

The modified one-pot process (R) [45] is often useful for systems with poor polyaddition reactivity. However, applicable only to highly soluble PI systems to avoid gelation or precipitation during the one-pot process. This process comprises the polycondensation in solution in the presence of catalysts, isolation of PI powder, redissolution of the PI powder in a fresh solvent, and the formation of PI films by solution casing. One-pot polycondensation was performed in a four-necked separable flask, equipped with a dry nitrogen gas inlet and outlet connected to a silicone oil-sealed bubbler, a condenser, Dean-Stark trap, and a specially designed mechanical stirrer (Nakamura Scientific Instruments Industry, UZ-SM1). This mixing apparatus has perfect sealability due to a non-contact magnetic coupling mechanism between an inner stirring rod and outer magnetic rotor. Diamine (2 mmol) and catalysts were dissolved at 100 °C in GBL in the afore-mentioned separable flask. After OHADA powder (2 mmol) was added to this solution in one portion, the reaction mixture with an initial total solid content of 30 or 40 wt% was rapidly heated to 200 °C and held for 4 h with continuous stirring in a nitrogen atmosphere. The reaction mixture was gradually diluted as appropriate with a minimum quantity of GBL during the reaction to ensure effective mechanical mixing. After the reaction, the fibrous PI powder was isolated from the homogeneous PI solutions and redissolved in fresh GBL. PI films were prepared via solution casting and annealing in the same manner as mentioned above (see the film preparation conditions via Route C). In some cases, the thermal conditions during the film preparation were optimized by fine tuning to obtain a better quality of PI films.

In this study, the chemical compositions of the PAA and PI systems are represented with the abbreviations of the monomer components used [tetracarboxylic dianhydrides (A) and diamines (B)] as A/B for homopolymers and A1;A2/B for copolymers.

2.2. Measurements

2.2.1. Structural Characterization of the Monomers and Polymers

The chemical structures of the synthesized monomers, their intermediates, and model compounds were characterized by FT-IR (KBr plate method, Jasco, Tokyo, Japan, FT-IR4100), ^{1}H-NMR and ^{13}C-NMR spectra (DMSO-d_6 or CDCl$_3$, JEOL, Tokyo, Japan, ECP400), and elemental analysis (J-Science Lab, Kyoto, Japan, Micro Corder JM10). Their melting thermograms were measured using DSC (Netzsch Japan, Yokohama, Japan, DSC3100) at a heating rate of 5 °C min^{-1} in a nitrogen atmosphere. The chemical structures of the PIs were characterized by FT-IR and ^{1}H-NMR spectroscopy.

2.2.2. Reduced Viscosities and Molecular Weights

The reduced viscosities (η_{red}) of the PIs and the corresponding PAAs, which can be virtually regarded as their inherent viscosities (η_{inh}), were measured at a solid content of 0.5 wt% at 30 °C on an Ostwald viscometer. The number- (M_n) and weight- (M_w) average molecular weights of highly soluble PIs in tetrahydrofuran (THF) were determined by gel permeation chromatography (GPC) using dehydrated THF as an eluent at room temperature on an HPLC system (Jasco, LC-2000 Plus) with a GPC column (Resonac, Tokyo, Japan, Shodex, KF-806L) at a flow rate of 1 mL min^{-1} with an ultraviolet-visible detector at 300 nm (Jasco, UV-2075). The calibration was performed using standard polystyrenes (Shodex, SM-105).

2.2.3. Linear Coefficients of Thermal Expansion (CTEs)

The CTE values of the PI specimens (15 mm long, 5 mm wide, and typically 20 μm thick) in the *X–Y* direction below the T_gs were measured by thermomechanical analysis (TMA) as an average in the range of 100–200 °C at a heating rate of 5 °C min^{-1}. The measurements were conducted at a fixed load (0.5 g per unit film thickness in μm, i.e., 10 g load for 20 μm-thick films) in a dry nitrogen atmosphere on a thermomechanical analyzer (Netzsch, TMA 4000). In this case, after the preliminary first heating run up to 120 °C and

subsequent cooling to room temperature in the TMA chamber, the data were collected from the second heating run to remove an influence of adsorbed water.

2.2.4. Heat Resistance

The glass transition temperatures (T_gs) of the PI films were determined from the peak temperature of the loss energy (E'') curves by dynamic mechanical analysis (DMA) at a heating rate of 5 °C min^{-1} on the TMA instrument (as before). The measurements were conducted under a sinusoidal load frequency of 0.1 Hz with an amplitude of 15 gf in a dry nitrogen atmosphere. The T_g was also determined from an inflection point of the TMA curve, where the specimens started to abruptly elongate, as an intersection of two tangential lines.

The thermal and thermo-oxidative stability of the PI films were evaluated from the 5% weight loss temperatures ($T_d{}^5$) by thermogravimetric analysis (TGA) on a thermo-balance (Netzsch Japan, Yokohama, Japan, TG-DTA2000). TGA was performed using a sample-charged and empty open aluminum pans in the range of 30–500 °C at a heating rate of 10 °C min^{-1} in a dry nitrogen and/or air atmosphere. A small weight loss due to the desorbed water around 100 °C during the heating run was compensated by off-set at 150 °C to 0% weight loss for the data analysis.

2.2.5. Optical Transparency

The light transmission spectra of the PI films (typically 20 μm thick) were measured on an ultraviolet-visible spectrophotometer (Jasco, V-530) in the wavelength (λ) range of 200–800 nm. The light transmittance at 400 nm (T_{400}) and the cut-off wavelength (λ_{cut}), at which the transmittance becomes substantially zero, were determined from the transmission spectra. The yellowness indices (YI, ASTM E 313) of the PI films were determined from the transmission spectra under a standard illuminant of D65 and a standard observer function of 2° using a color calculation software (Jasco) on the basis of the relationship:

$$YI = 100\,(1.2985x - 1.1335z)/y \tag{1}$$

where x, y, and z are the CIE tristimulus values. YI takes zero for an ideal white/transparent sample. The total light transmittance (T_{tot}, JIS K 7361-1) and diffuse transmittance (T_{diff}, JIS K 7136) of the PI films were measured on a double-beam haze meter equipped with an integrating sphere (Nippon Denshoku Industries, Tokyo, Japan, NDH 4000). The haze (turbidity) of the PI films was calculated from the relationship:

$$Haze = (T_{diff}/T_{tot}) \times 100 \tag{2}$$

2.2.6. Birefringence

The in-plane (n_{in}) and out-of-plane (n_{out}) refractive indices of the PI films were measured at 589.3 nm using a sodium lamp (D-line) on an Abbe refractometer (Atago, 4T, n_D range: 1.47–1.87), equipped with a polarizer using a contact liquid (sulfur-saturated methylene iodide n_D = 1.78–1.80) and a test piece (n_D = 1.92). The thickness-direction birefringence (Δn_{th}) of the PI films, which represents the relative extent of chain alignment in the X–Y direction, was calculated from the relationship:

$$\Delta n_{th} = n_{in} - n_{out} \tag{3}$$

2.2.7. Mechanical Properties

The tensile modulus (E), tensile strength (σ_b), and elongation at break (ε_b) of the PI specimens (film dimension: 30 mm long, 3 mm wide, typically 20 μm thick) were measured on a mechanical testing machine (A & D, Tensilon UTM-II) at a cross head speed of 8 mm min^{-1} at room temperature. The specimens ($n > 15$) were cut from high-quality film samples free of any defects such as fine bubbles. The data analysis was conducted using a data processing program (Softbrain, Tokyo, Japan, UtpsAcS Ver. 4.09).

2.2.8. Solubility Test

The solubility of the PIs was qualitatively estimated using their powder samples by observing whether the samples (10 mg) added in a solvent (1 mL) were completely dissolved without heating as the first step. When the samples were not completely dissolved at room temperature, they were heated at the established temperatures, and the state of dissolution was observed.

3. Results and Discussion

3.1. Approaches for Obtaining Colorless OHADA

3.1.1. Decolorization Processes of the OHADA Prototype

The OHADA prototype was intensely colored, as shown in Figure 5a. The thermally imidized film prepared using the OHADA prototype and 4,4′-ODA also exhibited an intense color (as shown later) owing to the presence of colored impurities contained in OHADA. The intense coloration of the PI films is a significant obstacle to their optical applications; therefore, complete decolorization of OHADA, which is also expected to further increase its chemical purity, is the key strategy for success of this study. The following approaches were conducted.
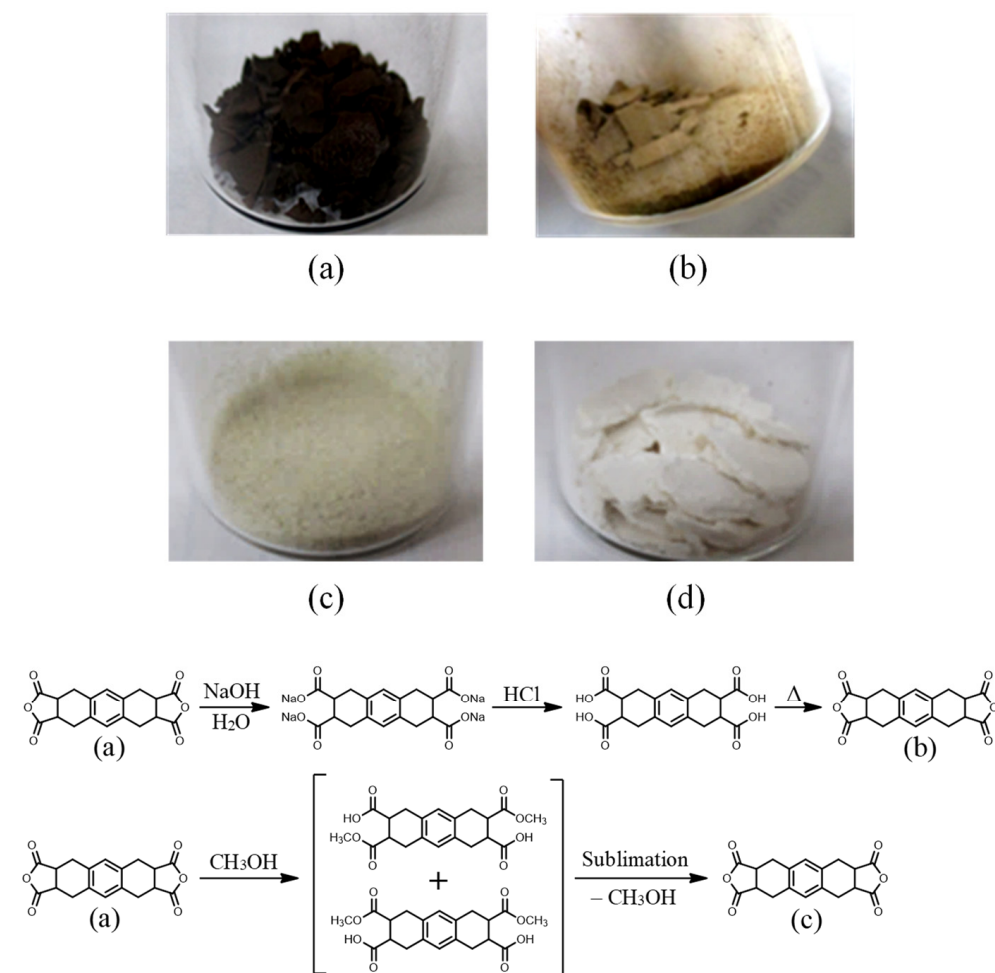

Figure 5. Appearance of OHADA obtained via different decolorization processes: (**a**) the product obtained after the Diels-Alder reaction in DMF (prototype), (**b**) the product obtained via alkaline hydrolysis of the prototype and subsequent neutralization, (**c**) the product obtained via half-esterification of the prototype and subsequent sublimation, and (**d**) the product obtained by recrystallization of the sublimated product (Method A).

(1) Activated carbon treatment

The addition of activated carbon, which preferentially adsorbs hydrophobic substances in polar adsorbents, to a DMF solution of the OHADA prototype was less effective in decolorizing the solution even after prolonged mild stirring at room temperature.

(2) Simple recrystallization

The OHADA prototype could be recrystallized from adequate solvents (Ac_2O, DMF, and GBL). However, simple recrystallization was less effective in significantly reducing the coloration of the precipitates.

(3) Alkaline hydrolysis of OHADA, neutralization, and cyclodehydration

The OHADA prototype was hydrolyzed with an NaOH aqueous solution and then neutralized with an HCl aqueous solution to convert the formed tetrasodium salt into the corresponding tetracarboxylic acid, followed by cyclodehydration by heating under vacuum. This process appreciably reduced the original coloration, although the product remained somewhat colored, as shown in Figure 5b.

(4) Half-esterification of OHADA and subsequent sublimation

The OHADA prototype did not sublimate even at elevated temperatures under vacuum. OHADA was therefore half-esterified by refluxing in a large excess of dehydrated methanol at the boiling point for 5 h and subsequent distilling off the excess of methanol. The product was sublimated at 250 °C under vacuum, accompanied by ring closure with the elimination of methanol. The unsublimated residue (OHADA formed via ring closure) was recycled for the half-esterification process as the first step. This process was effective in decolorizing OHADA. However, the sublimated product remained slightly colored, as shown in Figure 5c.

(5) Process (4) and subsequent recrystallization (Method A)

The sublimated product obtained via Process (4) was recrystallized from dehydrated GBL, and the precipitate formed was dried at 250 °C for 12 h under vacuum. This process provided the completely decolorized product, as shown in Figure 5d. The analytical data for this product are as follows. Melting point (DSC): 421 °C (single peak). FT-IR (KBr plate method, cm^{-1}): 3031 (C_{arom}–H stretching), 2972 (CH_2, C_{aliph}–H), 1840/1773 (acid anhydride, C=O). ^{1}H-NMR (400 MHz, DMSO-d_6, δ, ppm): 7.05 [s, 2H (2.00H), Ar–H], 3.72 [t (not well-resolved), 4H (4.01H), CH–C=O], 2.97–2.85 [m, 8H (8.02H), Ar–CH_2]. Elemental analysis, Anal. Calcd (%) for $C_{18}H_{14}O_6$ (326.31): C, 66.26; H, 4.32. Found: C, 66.01; H, 4.40. These results, which were not significantly different from those of the OHADA prototype, confirmed that the finally obtained white crystal is the desired product (OHADA), which probably has a further increased purity, as suggested by its melting point (421 °C) higher than that of the prototype (405 °C).

3.1.2. Simplified Process for Obtaining Colorless OHADA (Method B)

Assuming that the coloration of the OHADA prototype arises from some iodine-containing residues, the Diels-Alder reaction was conducted without NaI. However, virtually no reactions occurred.

The Diels-Alder reaction was also conducted at different temperatures (85, 120, and 140 °C) in the presence of NaI. The decrease in the reaction temperature tended to reduce the coloration of the product. However, it also increased the contents of some unknown impurities. The optimal conditions for obtaining the highest yield and purity of OHADA were determined to be 150 or 160 °C for 9 h. The high-temperature conditions were initially expected to favor the formation of the thermodynamic product of the Diels-Alder reaction rather than the kinetic product, as discussed later.

The effects of the solvent used in the Diels-Alder reactions were also investigated. No significant decolorization was observed in the reaction using *N,N*-dimethylacetamide (DMAc), which has a higher boiling point than DMF. On the other hand, the use of GBL significantly reduced the coloration of the crude product Figure 6a. However, subsequent thorough washing for removing colored impurities significantly decreased the yield (17–20%). After the Diels-Alder reaction in GBL, subsequent recrystallization of the crude

product from GBL (Method B) successfully afforded completely colorless product with a recrystallization yield of 80%, as shown in Figure 6b.
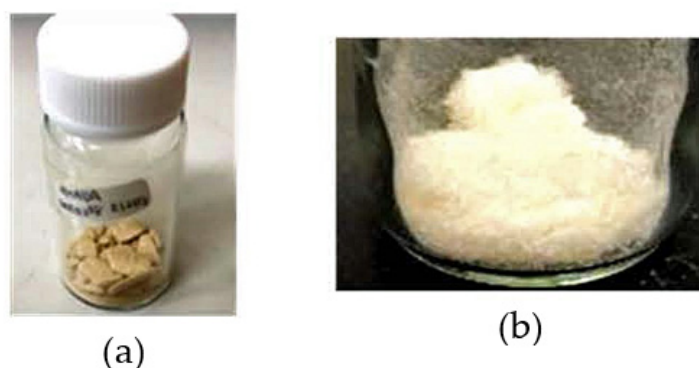

Figure 6. Appearance of OHADA at different stages: (**a**) the product obtained via the Diels-Alder reaction in GBL and (**b**) the product obtained by subsequent recrystallization from GBL (Method B).

Figure 7 shows the FT-IR spectrum of the colorless product obtained using Method B. The spectrum includes specific bands at 3032 (C_{arom}–H stretching), 2973/2917 (CH_2, C_{aliph}–H), and 1859(sh)/1841/1773 (acid anhydride, C=O). In addition, neither the COOH-related bands at ~2600 cm^{-1} (O–H stretching of hydrogen-bonded COOH groups) nor 1690 cm^{-1} (C=O stretching of hydrogen-bonded COOH) were observed in this spectrum. This indicates the absence of a hydrolyzed portion of the acid anhydride groups. These spectral features correspond with the desired structure, OHADA.
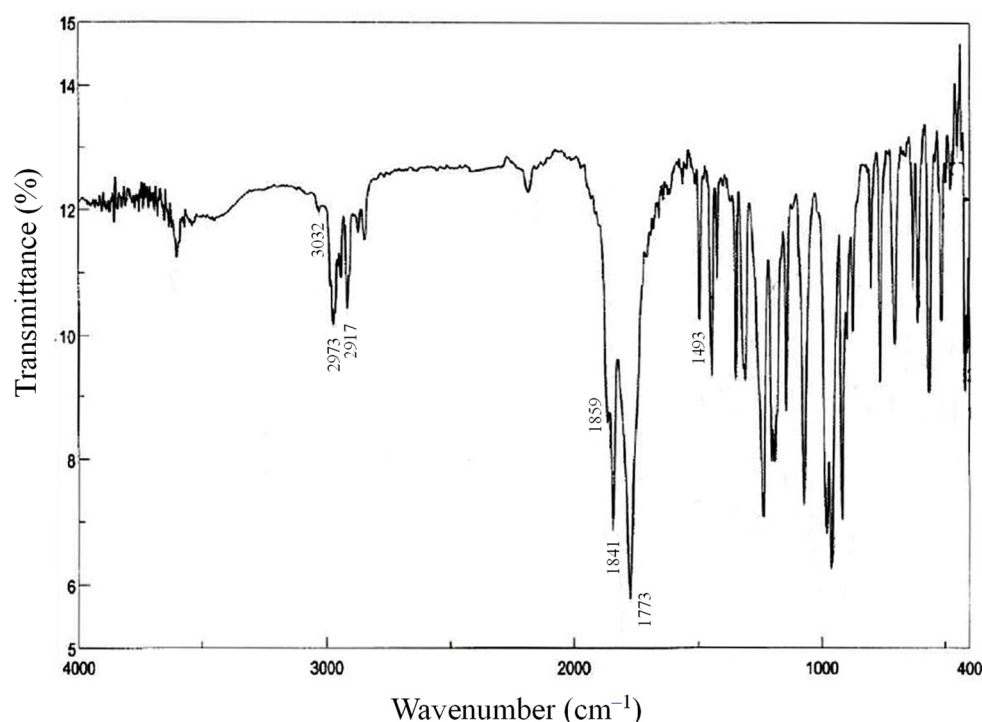

Figure 7. FT-IR spectrum (KBr plate method) of decolorized OHADA (Method B).

The ^{1}H-NMR spectrum of the colorless product (Method B) is shown in Figure 8. The following proton signals were observed: δ (ppm) = 7.04 [s, 2H (2.00H), Ar–H], 3.72 [t (not well-resolved), 4H (4.19H), J = 4.8 Hz, CH–C=O], 2.97–2.86 [m, 8H (8.14H), Ar–CH$_2$]. These spectral data were virtually identical to those of decolorized OHADA (Method A). The ^{13}C-NMR spectrum (100 MHz, DMSO-d_6) provided reasonable peaks: δ (ppm) = 175.5 (C$_1$),

134.6 (C_2), 127.5 (C_3), 41.1 (C_4), 29.1 (C_5) for the numbered carbon atoms of OHADA in Scheme 1.
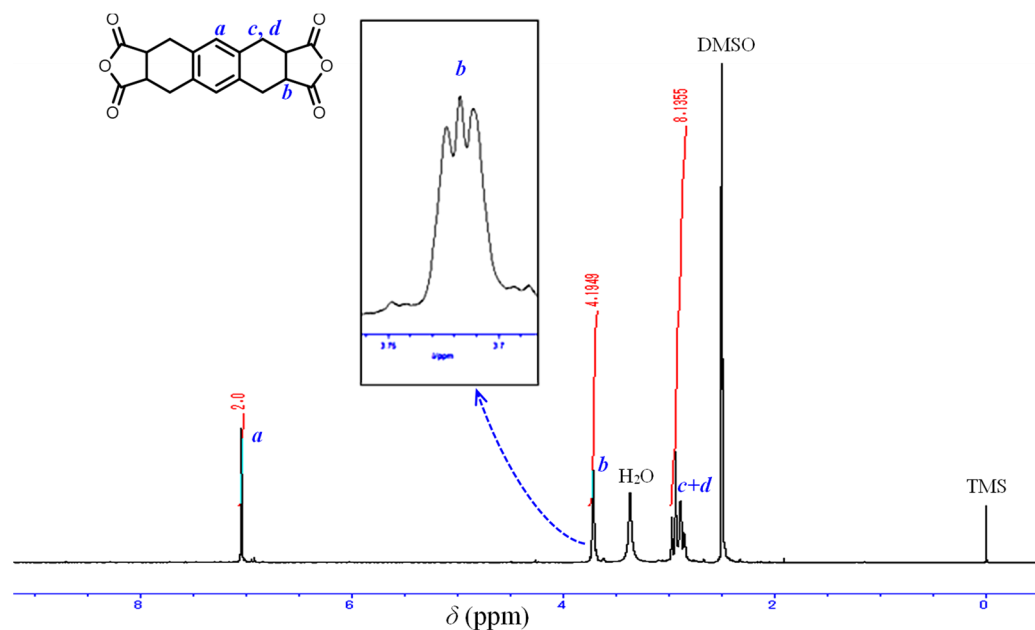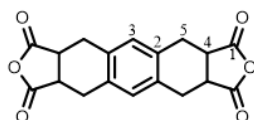

Figure 8. ^{1}H-NMR spectrum (400 MHz, DMSO-d_6) of decolorized OHADA (Method B).

Scheme 1. The numbering for the carbon atoms of OHADA.

The colorless product (Method B) also exhibited a relatively sharp, single endothermic peak for melting at 414 °C in the DSC thermogram (Figure 9), suggesting that the product is not the mixture of the stereoisomers of OHADA. The elemental analysis provided reasonable results: Anal. Calcd (%) for $C_{18}H_{14}O_6$ (326.31): C, 66.26; H, 4.32. Found: C, 66.00; H, 4.37). These analytical results confirmed that the colorless product (Method B) is OHADA with an extremely high chemical purity.
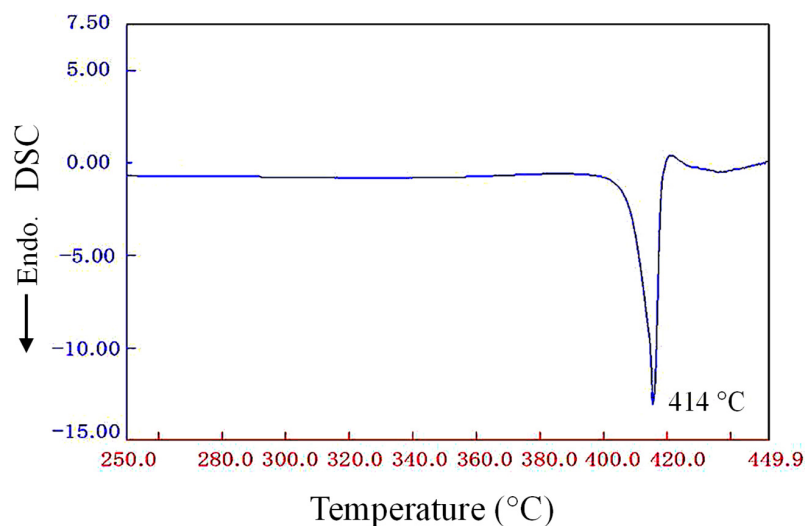

Figure 9. DSC thermogram of decolorized OHADA (Method B).

3.2. Estimated Steric Structure of OHADA

The steric structures of cycloaliphatic monomers are generally the key factors that dominate several properties (e.g., polymerizability, processability, and CTE) [31,33]. As shown in Figure 8, the proton signal at δ = 3.72 ppm (CH–C=O) of OHADA was observed as one triplet peak owing to coupling with the Ar–CH$_2$ protons with the relative integrated intensity corresponding to four protons (4H). This suggests that the four CH–C=O protons at δ = 3.72 ppm are all magnetically equivalent. In addition, the four C–C=O carbons in OHADA were also magnetically equivalent since the four C–C=O carbon signal was observed as the single peak at δ = 41.1 ppm. The steric structure of OHADA is therefore very likely to be one of the three candidates shown in Figure 10 (not the mixture).
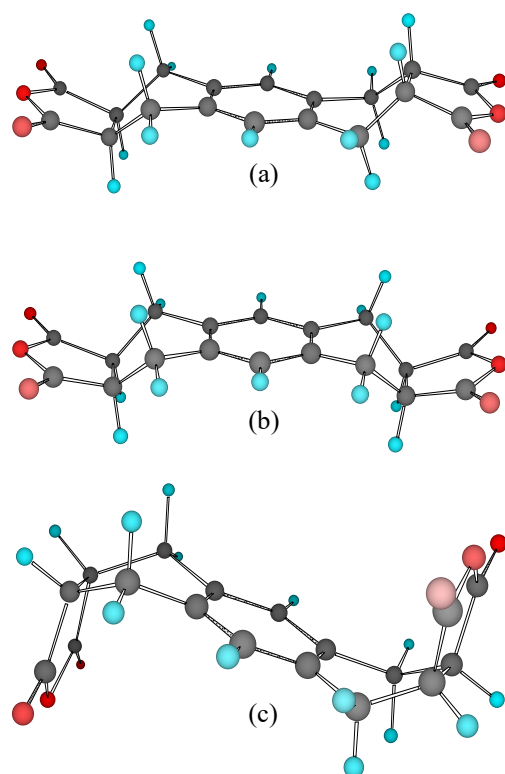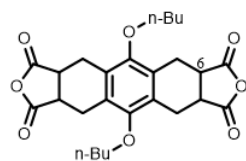

Figure 10. Possible steric structures of OHADA (CS-MOPAC): (**a**) *trans* bis-*exo*, (**b**) *cis* bis-*exo*, and (**c**) *trans* bis-*endo* form. Gray, light blue, and red balls represent C, H, and O elements, respectively.
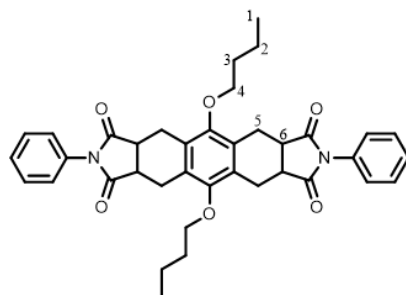
In the structure of OHADA, both cyclohexane units condensed to the central benzene unit most likely exist in the boat form since all four Ar–C$_{aliph}$ bonds must be in the same plane as the central benzene unit, as in durene; the chair form condensed to the benzene unit is very unlikely to exist due to its predicted high ring strain. The bis-*exo* form (Figure 10a,b) is the thermodynamic product. On the other hand, the bis-*endo* form (Figure 10c) is the kinetic product. If the present Diels-Alder reaction obeys the general "*endo* rule" [56], the *trans* bis-*endo* form (Figure 10c) is favored.

Kim et al. [54] synthesized an OHADA analog (1,9-di-*n*-butyloxy-substituted OHADA, Scheme 2) and its model compound (*N,N′*-diphenyl-diimide, Scheme 3) to speculate the steric structure of the former based on the HETCOR NMR spectrum [the correlation between the NMR signals of aliphatic carbons from C$_1$ to C$_6$ (Scheme 3) and the related proton signals (H$_1$–H$_6$)] of the latter; the model compound showed ^{13}C-NMR signals (CDCl$_3$) at δ = 75.3 (C$_4$), 40.1 (C$_6$), 32.7 (C$_3$), 23.4 (C$_5$), 19.9 (C$_2$), 14.4 (C$_1$) ppm. The C$_5$ signal at 23.4 ppm was correlated with the two proton signals (H$_5$, H$_5′$) at 3.61 and 2.76 ppm. On the other hand, the C$_6$ signal at 40.1 ppm correlated with the proton signal (H$_6$, s, broad) at 3.45 ppm, corresponding to the C$_6$ signal at 40.9 ppm (DMSO-d_6) and the H$_6$ signal (s, broad) at 3.75 ppm (DMSO-d_6) for the OHADA analog (Scheme 2). From the results, our

assignment mentioned above that the broad singlet or triplet proton signal at 3.72 ppm for OHADA comes from its CH–C=O proton is reasonable.

Scheme 2. Structure of an OHADA analog (1,9-di-*n*-butyloxy-substituted OHADA).

Scheme 3. Structure of a model compound of the OHADA analog.

On the basis of the HETCOR NMR spectrum, they speculated that the model compound, as well as the OHADA analog, probably has the steric structure of the *trans* bis-*endo* form. This agrees with the speculated steric structure of our OHADA (Figure 10c).

Unfortunately, our colorless OHADA was not suitable for determining its steric structure by single-crystal X-ray structure analysis. OHADA-based diimide compounds were then synthesized (Supplementary Materials Sections S1 and S2). However, crystal growth using the vapor diffusion method was unsuccessful.

3.3. Polyaddition Reactivity of OHADA with Aromatic Diamines

Table 1 summarizes the η_{red}-based polymerizability (polyaddition reactivity) of OHADA with aromatic diamines. Unexpectedly, the intensely colored OHADA prototype smoothly reacted with 4,4′-ODA (system #1p) and led to a viscous and homogeneous solution of PAA with a relatively high η_{red} value (0.88 dL g^{-1}), which was close to an approximate indication value of high molecular weights of PAAs ($\eta_{red} \geq$ ~1.0 dL g^{-1}). This result reflects the intrinsically high reactivity and a high chemical purity of the intensely colored OHADA prototype.

Table 1. Results of polyaddition of OHADA with aromatic diamines.

System No.	Grade of OHADA	Diamine	Solvent	Solid Content (Initial → Final) (wt%)	Appearance of PAA Solution	η_{inh} (PAA) (dL g^{-1})	PI Film Formability
1p	Colored (Prototype)	4,4′-ODA	NMP	50 → 12.5	Homogeneous and black	0.88	Sufficient
2p	Colored (Prototype)	TFMB	DMAc	50 → 11.5	Inhomogeneous and black	0.24	None (cracked)
1	Decolorized (Method A)	4,4′-ODA	NMP	30 → 17	Homogeneous and pale brown	1.32	Sufficient
3	Decolorized (Method A)	DABA	NMP	30 → 20	Homogeneous and dark brown	0.27	None (cracked)
4	Decolorized (Method A)	AB-TFMB	NMP	30	Inhomogeneous	—	—

A PAA with further enhanced η_{red} value (1.32 dL g^{-1}) was produced using colorless OHADA (Method A) (#1). The η_{red}-based polymerizability of colorless OHADA with

4,4′-ODA was compared with those of the related systems using other typical cycloaliphatic tetracarboxylic dianhydrides, as shown in Figure 11. OHADA showed somewhat lower reactivity with 4,4′-ODA than HTA-HQ (η_{red} = 2.32 dL g^{-1}). However, OHADA was much more reactive than H-PMDA (η_{red} = 0.57 dL g^{-1}). These results likely reflect the above-mentioned spacer effect based on the OHADA structure.

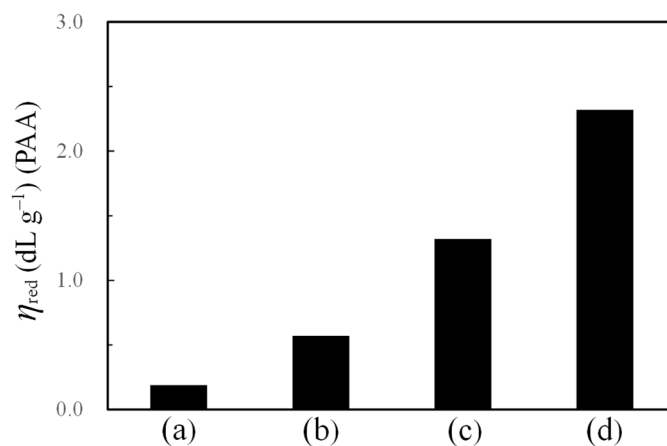**Figure 11.** The η_{red}-based relative polyaddition reactivity of various cycloaliphatic tetracarboxylic dianhydrides with 4,4′-ODA at the initial solid content of 30 wt% in DMAc or NMP at room temperature: (**a**) BTA, (**b**) H-PMDA, (**c**) OHADA, and (**d**) HTA-HQ.

On the other hand, polyaddition of OHADA and TFMB (#2), which is a limited diamine used in the production of colorless and low-CTE PIs, did not proceed smoothly and formed a slightly viscous solution containing an undissolved portion. The reasons for this insufficient polymerizability are unclear. Solution casting of the dissolved portion resulted in a brittle film with cracks.

The combination of OHADA and a typical amide-containing diamine with a rigid structure, 4,4′-diaminobenzanilide (DABA) (#3), formed a homogeneous PAA solution with a low η_{red} value (0.27 dL g^{-1}) corresponding to its poor film-forming ability. Another amide-containing diamine, AB-TFMB (Figure 3) (#4), behaved in a similar way to the TFMB system in that it also did not react smoothly with OHADA (the reaction mixture remained inhomogeneous even after prolonged stirring at room temperature).

3.4. Polymerizability of OHADA with Diamines during the Modified One-Pot Process

The modified one-pot process (R) [45] was applied to the OHADA/TFMB system due to the incompatibility with the conventional two-step process (T). One-pot polycondensation of OHADA and TFMB proceeded smoothly in GBL, consequently, a homogeneous and viscous PI solution was successfully obtained.

Figure 12 shows the FT-IR spectrum of the PI powder sample isolated from the homogeneous reaction mixture for the OHADA/TFMB system (R). This spectrum included the following specific bands (cm^{-1}): 3012 (C$_{arom}$–H stretching), 2956/2849 (C$_{aliph}$–H), 1786/1719 (imide, C=O), 1491 (1,4-phenylene), 1375 (imide, N–C$_{arom}$), 1312/1174 (C–F). In addition, neither the PAA specific bands at ~2600 cm^{-1} (hydrogen-bonded COOH, O–H stretching nor 1680/1530 cm^{-1} (amide, C=O stretching) were observed. The acid anhydride C=O stretching band at 1841 cm^{-1} was also not observed. These spectral features suggest that the imidization reaction was completed without the reverse reaction (depolymerization) by the one-pot process.
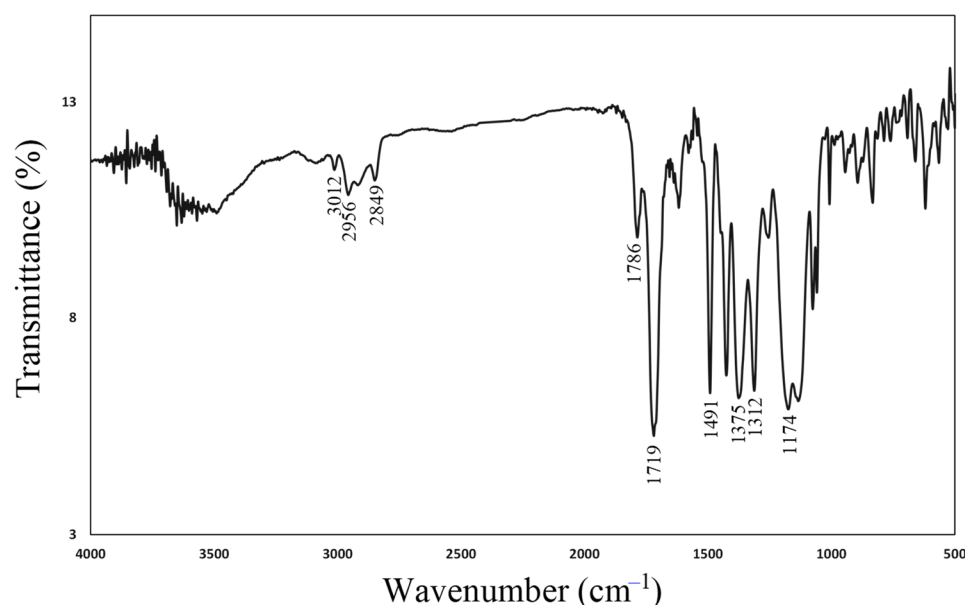
Figure 12. FT-IR spectrum (KBr plate method) of OHADA/TFMB polyimide (powder form) obtained via the modified one-pot process.

Figure 13 displays the ^{1}H-NMR spectrum of the OHADA/TFMB system (R) in DMSO-d_6. The traces of the unnecessary proton signals of the PAA-inherent COOH groups (δ = 12–13 ppm) and the NHCO groups ($\delta \sim 10.0$ ppm) were not observed. The spectrum was reasonable, corresponding to the expected PI structure. The progress of the polycondensation of OHADA and TFMB was also confirmed by GPC (M_w = 5.21 × 10^4, M_n = 1.89 × 10^4, Supplementary Materials Figure S1), although the PI had a somewhat low η_{red} value (0.51 dL g^{-1}). This PI exhibited sufficient film-forming ability. Thus, the modified one-pot process was the only applicable method to obtain flexible PI films from OHADA and TFMB.
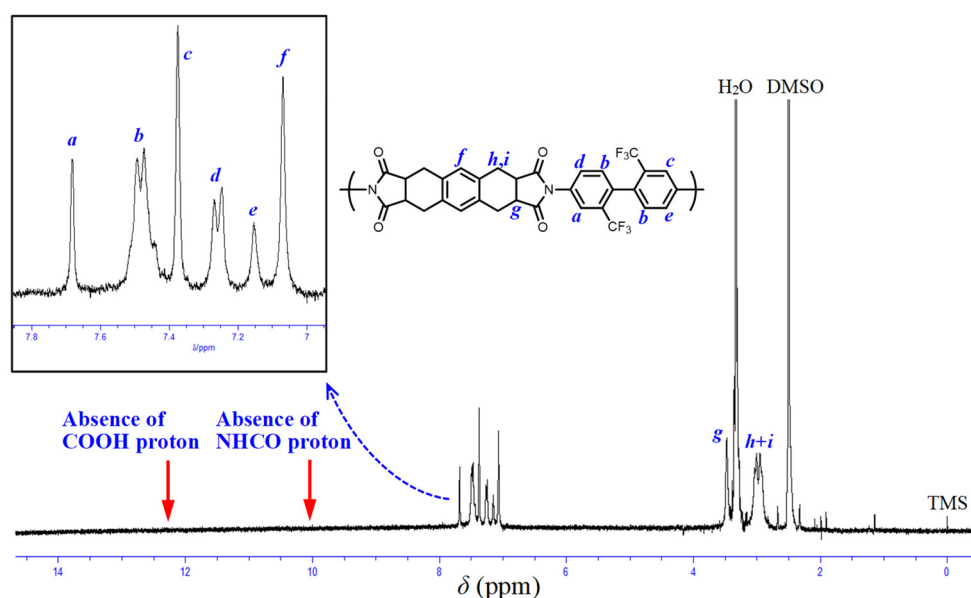

Figure 13. ^{1}H-NMR spectrum (DMSO-d_6) of OHADA/TFMB polyimide obtained via the modified one-pot process.

3.5. Solubility of OHADA-Based PIs

The results of the qualitative solubility tests of the OHADA-based PI powder samples are summarized in Table 2, in which the solvents are roughly arranged from the left in

order of their empirical dissolution power. The PI film (T) of CBDA/TFMB was insoluble in all of the examined solvents. In contrast, the PI powder sample (R) of OHADA/TFMB was soluble not only in common polar solvents (e.g., NMP, DMAc, DMF, and DMSO) but also less polar (less hygroscopic) solvents (e.g., GBL and triglyme) without heating. Even the copolymers prepared using CBDA, which often significantly reduces the solubility of the resultant PIs, showed excellent solubility, similar to the OHADA/TFMB system. The OHADA/AB-TFMB system (R) also exhibited excellent solubility, similar to the OHADA/TFMB system. These OHADA-based homo PIs afforded homogeneous and stable solutions with extremely high solid contents (30 wt%) in GBL. The observed excellent solubility in less hygroscopic solvents is advantageous in screen-printing applications to avoid the clogging of screen-printing plates due to the absorbed moisture into the inks.

Table 2. Results of solubility test using the PI powder samples obtained via the modified one-pot process.

No.	Tetracarboxylic Dianhydride	Diamine	NMP	DMAc	DMF	DMSO	GBL	CF	ACT	TriGL
			Heating Temperature (°C) at the 2nd Step							
			150	150	140	150	150	50	50	150
2	OHADA	TFMB	++	++	++	++	++	++	++	++
4	OHADA	AB-TFMB	++	++	++	++	++	−	−	++
7	CBDA (50) OHADA (50)	TFMB	++	++	++	++	++	−	+	++
8	CBDA (25) OHADA (75)	TFMB	++	++	++	++	++	−	++	++

(++) Soluble without heating, (+) soluble when heated at established temperatures and homogeneous after cooling to room temperature, and (−) insoluble even after heating. CF = chloroform, ACT = acetone, TriGL = triglyme.

3.6. Properties of OHADA-Based PI Films

3.6.1. Effect of OHADA Decolorization

Table 3 summarizes the properties of the OHADA-based PI films. Thermal imidization of the PAA film obtained from the OHADA prototype and 4,4′-ODA (#1p) produced a ductile film with a relatively high T_d^5 (N$_2$) close to 500 °C and a very high T_g exceeding 300 °C, despite the incorporated flexible ether linkages. This T_g was higher than that of the related PI derived from 4,4′-ODA and a typical rigid aromatic tetracarboxylic dianhydride, 3,3′,4,4′-biphenyltetracarboxylic dianhydride (s-BPDA) (T_g = 260 °C [57]). The enhanced T_g of OHADA/4,4′-ODA can be explained by the absence of rotatable single bonds in the OHADA structure, in contrast to HTA-HQ. However, this PI film (#1p) was intensely colored, as illustrated by the ultraviolet-visible transmission spectrum and appearance of the film in Figure 14. This intense color is a consequence of the use of the intensely colored OHADA, suggesting that not only ensuring the extremely high chemical purity but also complete decolorization of OHADA are unavoidable for the present purpose. In contrast, the use of decolorized OHADA (#1) provided a colorless PI film without haze via the two-step process (T), as shown in Figure 14. The properties of this colorless PI film were virtually equivalent to those of its colored counterpart, with the exception of the optical transparency.

Table 3. Film properties of OHADA-based PIs and a comparative system.

No.	Diamine	η_{red} (dL g^{-1})	Route	T_{400} (%)	YI	λcut (nm)	T_{tot} (%)	Haze (%)	Δn_{th}	T_g (°C)	CTE (ppm K^{-1})	E (GPa)	ε_b ave/max (%)	σ_b (GPa)	T_d^5 (N$_2$) (°C)	T_d^5 (air) (°C)
1p		0.88 [a] (NMP)	T	6.1	51.4	392	74.9	5.64	0.004	310 [c] 304 [d]	53.5				495	459
1	4,4′-ODA	1.32 [a] (NMP)	T	76.4	4.8	314	88.3	1.02	0.005	316 [c] 306 [d]	52.5	2.58	4.0/5.5	0.060	478	446
1		0.77 [b] (GBL)	C	74.7	2.4	316	88.8	0.86	0.006	290 [c] 290 [d]	53.8				—	—

Table 3. *Cont.*

No.	Diamine	η_{red} (dL g^{-1})	Route	T_{400} (%)	YI	λcut (nm)	T_{tot} (%)	Haze (%)	Δn_{th}	T_g (°C)	CTE (ppm K^{-1})	E (GPa)	ε_b ave/max (%)	σ_b (GPa)	$T_d{}^5$ (N$_2$) (°C)	$T_d{}^5$ (air) (°C)
2	TFMB	0.51 [b] (GBL)	R	82.4	2.7	293	89.5	2.77	0.013	304 [c] 298 [d]	59.9	3.31	3.3/4.7	0.084	512	433
4	AB-TFMB	0.59 [b] (GBL)	R	76.3	4.6	337	88.5	3.1	0.028	355 [c]	48.7 41.5 [e]	3.09	6.1/9.4	0.078	463	422
9 [f]	TFMB	1.24 [b] (GBL)	R	86.9	1.9	299	90.7	0.51	0.016	340 [d]	57.1	3.13	7.4/8.9	0.13	468	433

[a] Data of the PAAs. [b] Data of the PIs. [c] Data determined by TMA. [d] Data determined by DMA. [e] Data obtained via the multi-step slow drying process [initial rough drying at 65 °C for 2 h in an air convection oven + vacuum-drying at elevated temperatures on substrates (100 °C for 0.5 h + 150 °C for 0.5 h + 200 °C for 0.5 h + 250 °C for 1 h)] and subsequent annealing at 250 °C for 1 h under vacuum without the substrates. [f] H-PMDA/TFMB system [45].
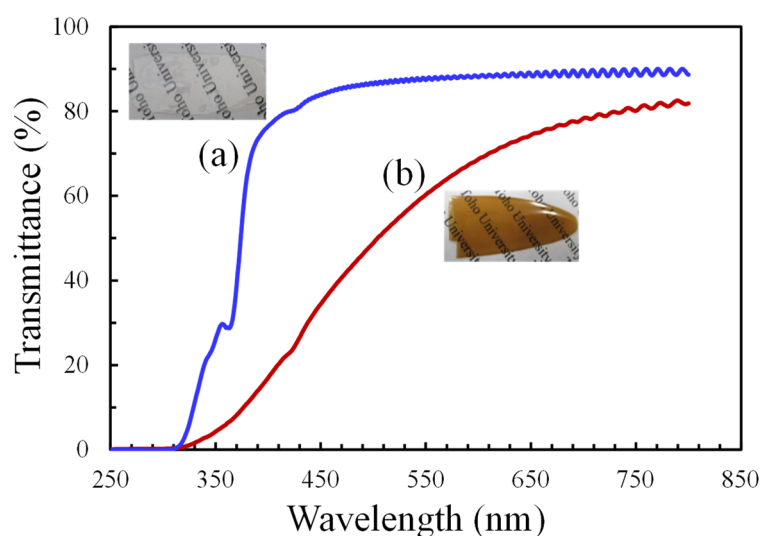

Figure 14. Ultraviolet-visible transmission spectra of the OHADA/4,4′-ODA PI films (20 μm thick, T) obtained using decolorized (Method A) (**a**) and colored OHADA (**b**). The insets are the appearance of each PI film specimen.

3.6.2. Features of the Properties of OHADA-Based PIs

The OHADA/4,4′-ODA system (#1) was suitable for the chemical imidization process. The isolated PI powder after chemical imidization was highly soluble in numerous solvents and afforded a homogeneous, stable GBL solution with a high solid content (18 wt%). Solution casting produced a colorless PI film with high heat resistance, similar to its thermally imidized counterpart (#1). Regardless of the preparation routes (T or C), the OHADA/4,4′-ODA film did not exhibit low CTE. This is related to the absence of main chain alignment in the *X–Y* direction (in-plane orientation), corresponding to their very low Δn_{th} values (0.005–0.006). It is widely accepted that in-plane chain orientation can be more prominently induced, particularly in PI systems comprising rigid, linear main chains, during the thermal imidization of PAA films fixed on substrates [58] or during solution casting [39,45]. The use of flexible monomers such as 4,4′-ODA, which significantly reduces the chain linearity, often disturbs the in-plane orientation behavior, as in the OHADA/4,4′-ODA system.

The OHADA/4,4′-ODA system (#1) has a sufficiently high molecular weight and rotational flexibility of the main chains to allow chain entanglement. Nonetheless, this PI film was not particularly tough (ε_b < 10%), likely owing to the peculiar steric structure of the OHADA-based diimide (OHADI) units in the main chains, which can disturb chain slippage [59] during the tensile testing.

The use of TFMB (#2) with a rigid and linear structure afforded a colorless PI film via the modified one-pot process. A feature of this PI was observed in its thermal stability.

Figure 15a compares the $T_d{}^5$ (N_2) values of the related PIs derived from a fixed diamine (TFMB) and different cycloaliphatic tetracarboxylic dianhydrides. The thermal stability increased in the following order: HTA-HQ/TFMB < CBDA/TFMB < H-PMDA/TFMB << OHADA/TFMB. The lowest thermal stability of the HTA-HQ/TFMB film is related to the presence of ester groups with relatively low bonding energies [60]. The relatively low thermal stability of the CBDA/TFMB film is probably ascribed to ring strain in the central cyclobutane unit of the CBDA structure. The higher thermal stability of the H-PMDA/TFMB film (#9) than that of its CBDA-based counterpart results from the central six-membered cyclohexane unit without ring strain in the former. The highest thermal stability of the OHADA/TFMB film is likely related to the condensed structure of the two cyclohexane units and the central benzene unit in the OHADA structure.
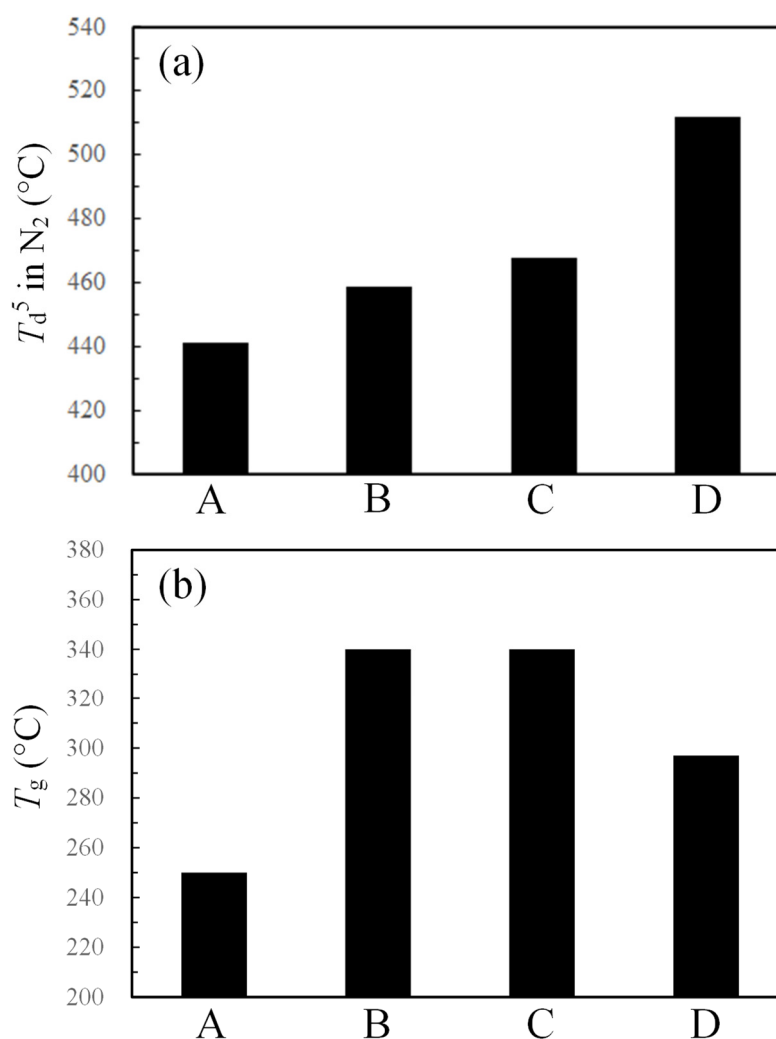

Figure 15. The $T_d{}^5$ in N_2 (**a**) and T_g (by DMA) (**b**) of the PI films obtained from TFMB and various cycloaliphatic tetracarboxylic dianhydrides: (A) HTA-HQ, (B) CBDA, (C) H-PMDA, and (D) OHADA.

Figure 15b compares the T_gs of the TFMB-based PIs. T_g is generally affected by a combination of the rotational barrier, intermolecular force, and chain stacking. The HTA-HQ/TFMB film exhibited the lowest T_g due to the presence of rotatable single bonds in the HTA-HQ-based diimide units. The OHADA/TFMB film showed a higher T_g than its HTA-HQ-based counterpart. However, it was lower than that of its H-PMDA-based counterpart (#9, Table 3). This can be explained by the fact that the OHADA/TFMB system has a lower content of the imide C=O groups than its H-PMDA-based counterpart. The dipole-dipole interactions between the imide C=O groups are believed to be the origin of

strong intermolecular force of PIs [61,62]. In addition, if OHADA has the *trans* bis-*endo* structure (it is highly likely), as depicted in Figure 10c, it disturbs close chain stacking. Nonetheless, the OHADA/TFMB film maintained a quite high T_g close to 300 °C. This probably reflects the absence of rotatable single bonds in the structure of OHADA, in contrast to HTA-HQ.

Figure 16 displays schematically drawn extended chains of the OHADA/TFMB and related systems. Empirically, when the extended chain looks highly linear, the corresponding real PI film generates a low CTE almost without exception [33,45,63–65]. The CBDA/TFMB system (Figure 16A) is a representative case, in which a crank-shaft-like relatively linear chain form resulted in a low CTE (21 ppm K^{-1} [32]). If OHADA has the crank-shaft-like steric structure shown in Figure 10a, as in CBDA, the corresponding real OHADA/TFMB film is expected to generate a low CTE due to its predicted linear extended chains (Figure 16B), as in the CBDA/TFMB system. By contrast, when the extended chain has a significantly meandered form, the corresponding real PI film usually shows a greatly increased CTE. The H-PMDA/TFMB system [#9, Figure 16C] is a typical case, which exhibited indeed a high CTE (57 ppm K^{-1} [45]). If OHADA has the *trans* bis-*endo* structure (it is highly likely) (Figure 10c), the extend chain will become a significantly meandered form, as shown in Figure 16D, which is disadvantageous for achieving low CTE property. This hypothesis corresponds to the fact that the OHADA/TFMB film (#2) did not exhibit a low CTE.
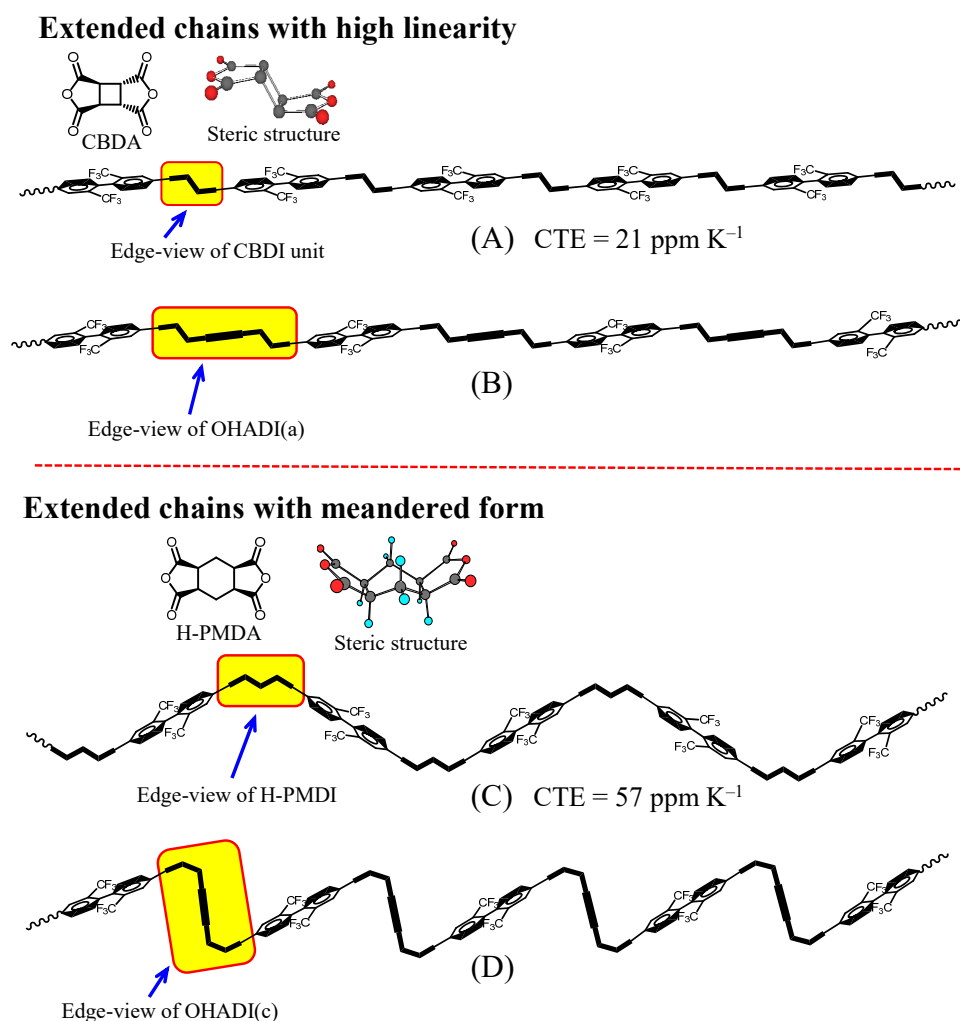
Extended chains with high linearity

(A)   CTE = 21 ppm K^{-1}

(B)

Extended chains with meandered form

(C)   CTE = 57 ppm K^{-1}

(D)

Figure 16. Schematic drawings of the extended PI chains with high linearity and meandered form: (**A**) CBDA/TFMB, (**B**) OHADA(a)/TFMB, (**C**) H-PMDA/TFMB, and (**D**) OHADA(c)/TFMB. For simplicity, the diamine is fixed to a typical rigid diamine, TFMB.

The CTEs of PI films tend to gradually decrease with increasing molecular weight of the PIs [33]. Therefore, there is a chance of lowering the CTE of OHADA/TFMB a little more. However, as long as the steric structure of OHADA is the significantly distorted *trans* bis-*endo* form (Figure 10c), achieving any significant reduction in the CTEs by enhancing the molecular weight of the PIs is unlikely.

As the next approach, a rigid amide-type diamine, AB-TFMB (Figure 3), which was effective to reduce the CTEs [44,45], was used. The solution homogeneity of the OHADA/AB-TFMB system (#4) was maintained during the modified one-pot process, whereas the related system (CBDA/AB-TFMB) underwent gelation during chemical imidization [44]. These results emphasize again the significant solubility-improving effect of OHADA. The isolated PI powder of OHADA/AB-TFMB afforded a homogeneous and stable GBL solution with a very high solid content (30 wt%). Solution casting produced a ductile and highly transparent PI film with a significantly enhanced T_g (355 °C) relative to that of OHADA/TFMB (#2, 304 °C). This likely reflects the effect of intermolecular hydrogen-bonding between the incorporated amide groups.

A certain degree of effect of AB-TFMB on reducing the CTE was observed; the OHADA/AB-TFMB film (#4) exhibited a somewhat decreased CTE (48.7 ppm K^{-1}), compared with that of the OHADA/TFMB film (59.9 ppm K^{-1}). Our previous study [33] revealed that a slow drying process during the solution casting was somewhat effective in reducing the CTE. The OHADA/AB-TFMB cast film prepared by slow drying (the detailed conditions are provided in the footnote of Table 3) exhibited a further reduced CTE (41.5 ppm K^{-1}).

3.6.3. Another Feature: Thermoplasticity

The thermoplasticity of the OHADA-based PIs was evaluated using DMA. We demonstrated previously that the thermoplasticity of PI films, which is closely related to the steepness of the glass transition, can be evaluated by an index (i.e., a maximum slope ($-d \log E'/dT$), above the T_g in the storage modulus (E') curve on DMA (frequency: 0.1 Hz)) [66]. For example, an injection-moldable bisphenol A-type poly(ether imide), ULTEM1000 [67], showed a very high thermoplasticity index ($-d \log E'/dT = 0.65$), whereas a typical non-thermoplastic PI, *s*-BPDA/*p*-phenylenediamine, had a very low thermoplasticity index (0.008).

Figure 17 shows the DMA curves of the OHADA/TFMB film (#2, R), together with those of the CBDA/TFMB system (T) for comparison. The OHADA/TFMB film exhibited an abrupt reduction in the E' curve above the T_g without the rubbery plateau region, as shown in Figure 17a. This corresponds to its high thermoplasticity index (0.21). This result is likely related to the disrupted close chain stacking and concomitantly weakened intermolecular forces. In contrast, the E' curve of the CBDA/TFMB film gradually decreased above the T_g (Figure 17b), corresponding to its much lower thermoplasticity index (0.030). This reflects its crank-shaft-like, relatively linear chain structure.

These features observed in the OHADA/TFMB system (i.e., the combined properties (non-coloration + high T_g + excellent thermoplasticity and solubility)) are almost unprecedented among optically transparent PIs. This is probably ascribed to the unique (ladder-like + highly distorted) steric structure of OHADA.

3.6.4. Modification of CBDA/TFMB Using OHADA as the Comonomer

The CBDA/TFMB system is known to achieve high optical transparency and a low CTE [32]. The two-step process (T) was the only method for forming its free-standing PI film. Indeed, the one-pot process was unsuccessful in the case of this system due to gelation, as shown in Supplementary Materials Figure S2. If the solubility of this system was dramatically improved, and consequently, the one-pot or chemical imidization process became applicable, there is a good chance of a further significant decrease in the CTE [44], while maintaining the high optical transparency inherent in the CBDA/TFMB system.
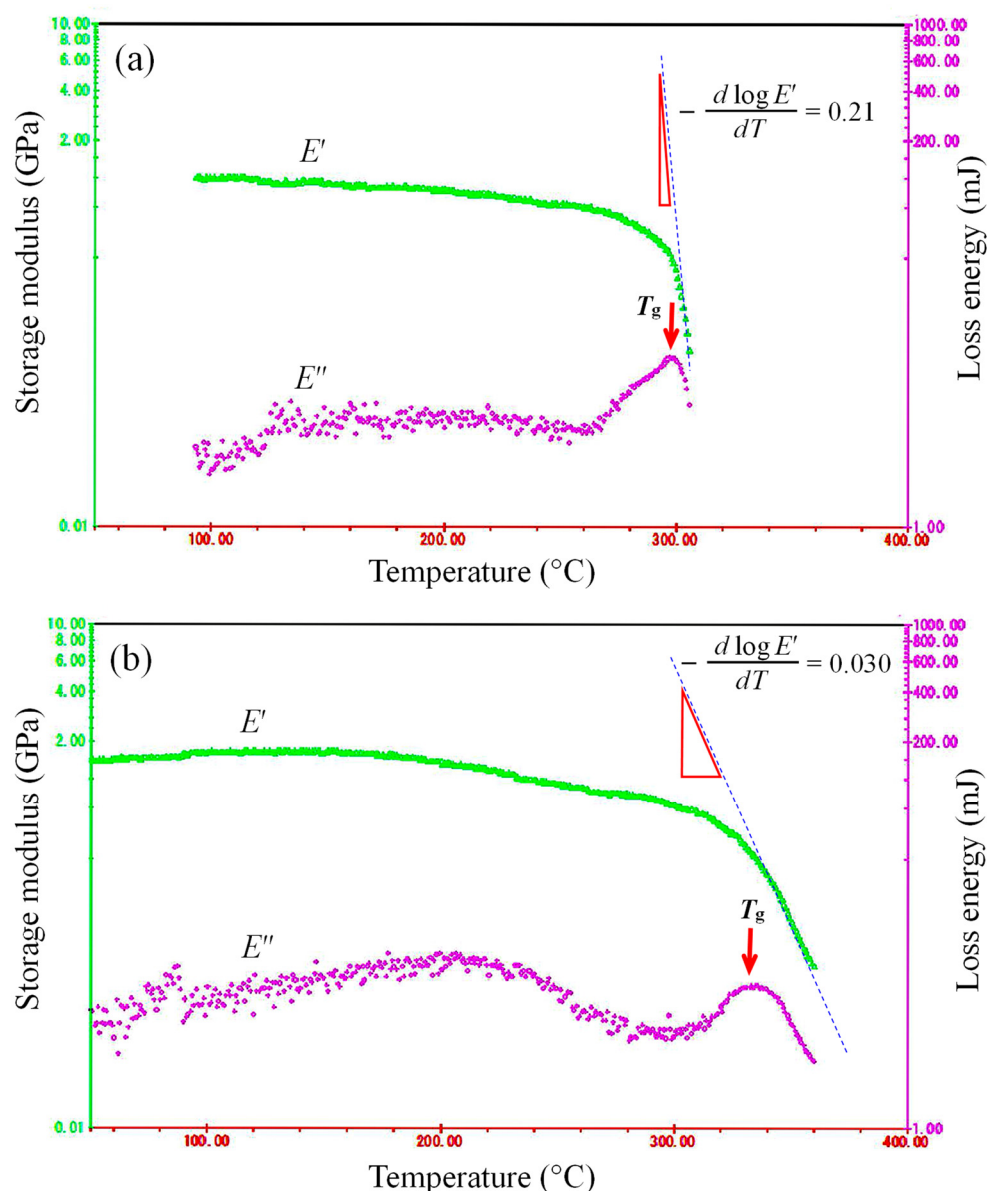
Figure 17. DMA curves and thermoplasticity indices ($-d \log E'/dT$) of the PI films: (**a**) OHADA/TFMB and (**b**) CBDA/TFMB systems.

To modify the CBDA/TFMB system, OHADA, which was proved to exert a strong solubility-improving effect without sacrificing its originally high transparency, as mentioned above, was used as the comonomer. The results of this approach are summarized in Table 4. However, copolymerization with a minor content of OHADA (25 mol%) was ineffective in preventing gelation during the modified one-pot process. On the other hand, increasing the OHADA content to 50 (#7) and 75 mol% (#8) produced homogeneous PI solutions in GBL with enhanced η_{red} values. Despite the use of CBDA (25 and 50 mol%), the isolated PI powder samples were highly soluble in common solvents (Table 2) and afforded homogeneous and stable GBL solutions with a high solid content (20 wt%). The cast films of the copolymers (#7, 8) exhibited T_gs approximately 30 °C higher than that of the OHADA/TFMB film (#2), as speculated from the general additivity rule in the T_g–copolymer composition relationship. The CTE–copolymer composition relationship is also well described by the additivity rule [44]. However, the measured CTEs of the present copolymers were much higher than those estimated using the additivity rule. This is probably ascribed to an overwhelming orientation-randomizing effect of OHADA, which

arises from its predicted highly distorted steric structure. The copolymer films were not very tough ($\varepsilon_b < 5\%$). However, they maintained a degree of ductility, as suggested by the fact that they were not broken by the simple folding test, during which the films were folded with a virtually zero curvature radius.

Table 4. Film properties of CBDA/TFMB-based copolymers (R) modified with OHADA.

No.	CBDA (mol%)	OHADA (mol%)	η_{red} (PI) (dL g^{-1})	T_{400} (%)	YI	λcut (nm)	T_{tot} (%)	Haze (%)	Δn_{th}	T_g [a] (°C)	CTE (ppm K^{-1})	E (GPa)	ε_b ave/max (%)	σ_b (GPa)	$T_d{}^5$ (N$_2$) (°C)	$T_d{}^5$ (air) (°C)
5	100	0	Gelation during the modified one-pot process in GBL													
6	75	25	Gelation during the modified one-pot process in GBL													
7	50	50	0.98 (GBL)	76.5	7.1	271	82.2	3.21	0.015	333	56.9	3.02	3.4/4.9	0.080	448	436
8	25	75	0.89 (GBL)	69.3	10.5	261	78.4	4.43	0.014	323	58.8	2.94	3.6/4.8	0.086	461	409

[a] Data determined by TMA.

4. Conclusions

A novel cycloaliphatic tetracarboxylic dianhydride (OHADA) was synthesized via the tetra-bromination of durene and subsequent Diels-Alder reaction of the resulting tetra-bromide and maleic anhydride to overcome the poor flexibility of structural modification and property improvement of colorless PIs. The OHADA prototype had a sufficiently high chemical purity, although it was intensely colored. The OHADA prototype exhibited high polyaddition reactivity with 4,4′-ODA and formed a PAA with a relatively high molecular weight. However, thermal imidization of the PAA cast film resulted in an intensely colored PI film.

To completely remove the intense coloration of this PI film, the decolorization of OHADA was thoroughly examined, and colorless OHADA with a very high purity was successfully obtained. The ^{1}H-NMR spectrum suggested that the steric structure of OHADA was one of the three candidates (*trans* bis-*exo*, *cis* bis-*exo*, and *trans* bis-*endo* form); according to the general "*endo* rule" of the Diels-Alder reaction, the most plausible steric structure of OHADA is the significantly distorted *trans* bis-*endo* form.

Equimolar polyaddition of decolorized OHADA with 4,4′-ODA in NMP at room temperature produced a high-molecular-weight PAA with an enhanced η_{red} value (1.32 dL g^{-1}). Thermal imidization of the PAA cast film afforded a colorless PI film with a very high T_g in excess of 300 °C, despite the high rotational flexibility of the 4,4′-ODA structure. This unexpectedly high T_g was ascribed to the absence of rotatable single bonds in the OHADA structure. The chemical imidization process was applicable to the OHADA/4,4′-ODA system without gelation or precipitation during the reaction.

On the other hand, the polyaddition of OHADA and TFMB did not proceed smoothly; specifically, an undissolved portion remained in the reaction mixture even after prolonged stirring. In contrast, the modified one-pot polycondensation of OHADA and TFMB enabled the polymerization to proceed, yielding a homogeneous and viscous PI solution. The isolated PI powder, as well as those of the other OHADA-based PIs examined, was highly soluble in numerous solvents and afforded a homogeneous, stable GBL solution with a very high solid content (30 wt%). Solution casting provided a ductile and colorless OHADA/TFMB PI film with a very high T_g close to 300 °C. The $T_d{}^5$ (N$_2$) of this system was remarkably high compared with those of other related TFMB-derived semi-cycloaliphatic PIs. However, contrary to our expectations, the OHADA/TFMB film did not exhibit a low CTE. This PI film also exhibited excellent thermoplasticity, likely reflecting the unique (ladder-like + highly distorted) steric structure of OHADA.

The combination of amide-containing AB-TFMB and OHADA achieved a significantly enhanced T_g (355 °C) and a somewhat reduced CTE (41.5 ppm K^{-1}) while maintaining high optical transparency and excellent solubility.

The CBDA/TFMB system, which can only be produced through the conventional two-step process, was modified via copolymerization with OHADA. This approach afforded copolymers compatible with the one-pot process with significantly improved solubility while maintaining excellent optical transparency and very high T_gs.

Thus, OHADA enabled the development of new solution-processable colorless PIs with excellent combined properties for applications as potential optoelectronic materials.

References

1. Sumitomo Chemical Co., Ltd., Poly(ether sulfone). Available online: http://www.sumitomo-chem.co.jp/sep/english/products/pes/index.html (accessed on 20 March 2023).
2. Cassidy, P.E. *Thermally Stable Polymers: Syntheses and Properties*; Marcel Dekker: New York, NY, USA, 1980.
3. Mittal, K.L. (Ed.) *Polyimides: Synthesis, Characterization, and Applications*; Plenum Press: New York, NY, USA, 1984; Volume 1–2.
4. Bessonov, M.I.; Koton, M.M.; Kudryavtsev, V.V.; Laius, L.A. (Eds.) *Polyimides: Thermally Stable Polymers*; Plenum: New York, NY, USA, 1987.
5. Feger, C.; Khojasteh, M.M.; McGrath, J.E. (Eds.) *Polyimides: Materials, Chemistry and Characterization*; Elsevier Science Publishers: Amsterdam, The Netherlands, 1989.
6. Sroog, C.E. Polyimide. *Prog. Polym. Sci.* **1991**, *16*, 561–694. [CrossRef]
7. Abadie, M.J.M.; Sillion, B. (Eds.) *Polyimides and Other High-Temperature Polymers*; Elsevier Science Publishers: Amsterdam, The Netherlands, 1991.
8. Bessonov, M.I.; Zubkov, V.A. (Eds.) *Polyamic Acid and Polyimides: Synthesis, Transformation and Structure*; CRC Press: Boca Raton, FL, USA, 1993.
9. Feger, C.; Khojasteh, M.M.; Htoo, M.S. (Eds.) *Advances in Polyimide Science and Technology*; Technomic Publishing: Lancaster, PA, USA, 1993.
10. Ghosh, M.K.; Mittal, K.L. (Eds.) *Polyimides: Fundamentals and Applications*; Marcel Dekker: New York, NY, USA, 1996.
11. Sachdev, H.S.; Khojasteh, M.M.; Feger, C. (Eds.) *Advances in Polyimides and Low Dielectric Polymers*; Society of Plastic Engineers: New York, NY, USA, 1997.
12. Hergenrother, P.M. The Use, design, synthesis, and properties of high performance/high temperature polymers: An overview. *High Perform. Polym.* **2003**, *15*, 3–45. [CrossRef]
13. Ree, M. High performance polyimides for applications in microelectronics and flat panel displays. *Macromol. Res.* **2006**, *14*, 1–33. [CrossRef]
14. Ando, S.; Ueda, M.; Kakimoto, M.; Kochi, M.; Takeichi, T.; Hasegawa, M.; Yokota, R. (Eds.) *The Latest Polyimides: Fundamentals and Applications*, 2nd ed.; NTS: Tokyo, Japan, 2010.
15. Liaw, D.J.; Wang, K.L.; Huang, Y.C.; Lee, K.R.; Lai, J.Y.; Ha, C.S. Advanced polyimide materials: Syntheses, physical properties and applications. *Prog. Polym. Sci.* **2012**, *37*, 907–974. [CrossRef]

16. Tsai, C.L.; Yen, H.J.; Liou, G.S. Highly transparent polyimide hybrids for optoelectronic applications. *React. Funct. Polym.* **2016**, *108*, 2–30. [CrossRef]

17. Yang, S.Y. (Ed.) *Advanced Polyimide Materials: Synthesis, Characterization, and Applications*; Chemical Industry Press: Shanghai, China; Elsevier: Amsterdam, The Netherlands, 2018.

18. Diaham, S. (Ed.) *Polyimide for Electronic and Electrical Engineering Applications*; IntechOpen: London, UK, 2021.

19. Hasegawa, M.; Horie, K. Photophysics, photochemistry, and optical properties of polyimides. *Prog. Polym. Sci.* **2001**, *26*, 259–335. [CrossRef]

20. Matsuura, T.; Hasuda, Y.; Nishi, S.; Yamada, N. Polyimide derived from 2,2′-bis(trifluoromethyl)-4,4′-diaminobiphenyl. 1. Synthesis and characterization of polyimides prepared with 2,2′-bis(3,4-dicarboxyphenyl)hexafluoropropane dianhydride or pyromellitic dianhydride. *Macromolecules* **1991**, *24*, 5001–5005. [CrossRef]

21. Hasegawa, M.; Ishigami, T.; Ishii, J.; Sugiura, K.; Fujii, M. Solution-processable transparent polyimides with low coefficient of thermal expansion and self-orientation behavior induced by solution casting. *Eur. Polym. J.* **2013**, *49*, 3657–3672. [CrossRef]

22. Volksen, W.; Cha, H.J.; Sanchez, M.I.; Yoon, D.Y. Polyimides derived from nonaromatic monomers: Synthesis, characterization and potential applications. *React. Funct. Polym.* **1996**, *30*, 61–69. [CrossRef]

23. Seino, H.; Sasaki, T.; Mochizuki, A.; Ueda, M. Synthesis of fully aliphatic polyimides. *High Perform. Polym.* **1999**, *11*, 255–262. [CrossRef]

24. Mathews, A.S.; Kim, I.; Ha, C.S. Synthesis, characterization, and properties of fully aliphatic polyimides and their derivatives for microelectronics and optoelectronics applications. *Macromol. Res.* **2007**, *15*, 114–128. [CrossRef]

25. Tsuda, Y.; Etou, K.; Hiyoshi, N.; Nishikawa, M.; Matsuki, Y.; Bessho, N. Soluble copolyimides based on 2,3,5-tricarboxycyclopentyl acetic dianhydride and conventional aromatic tetracarboxylic dianhydrides. *Polym. J.* **1998**, *30*, 222–228. [CrossRef]

26. Ni, H.; Liu, J.; Wang, Z.; Yang, S. A review on colorless and optically transparent polyimide films: Chemistry, process and engineering applications. *J. Ind. Eng. Chem.* **2015**, *28*, 16–27. [CrossRef]

27. Suzuki, H.; Abe, T.; Takaishi, K.; Narita, M.; Hamada, F. The synthesis and X-ray structure of 1,2,3,4-cyclobutane tetracarboxylic dianhydride and the preparation of a new type of polyimide showing excellent transparency and heat resistance. *J. Polym. Sci. Part A Polym. Chem.* **2000**, *38*, 108–116. [CrossRef]

28. Matsumoto, T. Nonaromatic polyimides derived from cycloaliphatic monomers. *Macromolecules* **1999**, *32*, 4933–4939. [CrossRef]

29. Li, J.; Kato, J.; Kudo, K.; Shiraishi, S. Synthesis and properties of novel soluble polyimides having an unsymmetric spiro tricyclic dianhydride unit. *Macromol. Chem. Phys.* **2000**, *201*, 2289–2297. [CrossRef]

30. Hasegawa, M.; Kasamatsu, K.; Koseki, K. Colorless poly(ester imide)s derived from hydrogenated trimellitic anhydride. *Eur. Polym. J.* **2012**, *48*, 483–498. [CrossRef]

31. Hasegawa, M.; Hirano, D.; Fujii, M.; Haga, M.; Takezawa, E.; Yamaguchi, S.; Ishikawa, A.; Kagayama, T. Solution-processable colorless polyimides derived from hydrogenated pyromellitic dianhydride with controlled steric structure. *J. Polym. Sci. Part A Polym. Chem.* **2013**, *51*, 575–592. [CrossRef]

32. Hasegawa, M.; Horiuchi, M.; Kumakura, K.; Koyama, J. Colorless polyimides with low coefficient of thermal expansion derived from alkyl-substituted cyclobutanetetracarboxylic dianhydrides. *Polym. Int.* **2014**, *63*, 486–500. [CrossRef]

33. Hasegawa, M.; Fujii, M.; Ishii, J.; Yamaguchi, S.; Takezawa, E.; Kagayama, T.; Ishikawa, A. Colorless polyimides derived from 1*S*,2*S*,4*R*,5*R*-cyclohexanetetracarboxylic dianhydride, self-orientation behavior during solution casting, and their optoelectronic applications. *Polymer* **2014**, *55*, 4693–4708. [CrossRef]

34. Shiotani, A.; Shimazaki, H.; Matsuo, M. Preparation of transparent polyimides derived from *cis*- and *trans*-dicyclohexyl-3,3′,4,4′– tetracarboxylic dianhydrides. *Macromol. Mater. Eng.* **2001**, *286*, 434–441. [CrossRef]

35. Guo, Y.; Song, H.; Zhai, L.; Liu, J.; Yang, S. Synthesis and characterization of novel semi-alicyclic polyimides from methyl-substituted tetralin dianhydride and aromatic diamines. *Polym. J.* **2012**, *44*, 718–723. [CrossRef]

36. Fang, X.; Yang, Z.; Zhang, S.; Gao, L.; Ding, M. Synthesis and properties of polyimides derived from *cis*- and *trans*-1,2,3,4-cyclohexanetetracarboxylic dianhydrides. *Polymer* **2004**, *45*, 2539–2549. [CrossRef]

37. Jiang, G.; Wang, D.; Du, H.; Wu, X.; Zhang, Y.; Tan, Y.; Wu, L.; Liu, J.; Zhang, X. Reduced coefficients of linear thermal expansion of colorless and transparent semi-alicyclic polyimide films via incorporation of rigid-rod amide moiety. Preparation and properties. *Polymers* **2020**, *12*, 413. [CrossRef] [PubMed]

38. Zhuang, Y.; Seong, J.G.; Lee, Y.M. Polyimides containing aliphatic/alicyclic segments in the main chains. *Prog. Polym. Sci.* **2019**, *92*, 35–88. [CrossRef]

39. Hasegawa, M. Development of solution-processable, optically transparent polyimides with ultra-low linear coefficients of thermal expansion. *Polymers* **2017**, *9*, 520. [CrossRef]

40. Hu, X.; Yan, J.; Wang, Y.; Mu, H.; Wang, Z.; Cheng, H.; Zhao, F.; Wang, Z. Colorless polyimides derived from 2*R*,5*R*,7*S*,10*S*-naphthanetetracarboxylic dianhydride. *Polym. Chem.* **2017**, *8*, 6165–6172. [CrossRef]

41. Ozawa, H.; Ishiguro, E.; Kyoya, Y.; Kikuchi, Y.; Matsumoto, T. Colorless polyimides derived from an alicyclic tetracarboxylic dianhydride, CpODA. *Polymers* **2021**, *13*, 2824. [CrossRef]

42. Liu, H.; Zhai, L.; Bai, L.; He, M.; Wang, C.; Mo, S.; Fan, L. Synthesis and characterization of optically transparent semi-aromatic polyimide films with low fluorine content. *Polymer* **2019**, *163*, 106–114. [CrossRef]

43. Hu, X.; Mu, H.; Wang, Y.; Wang, Z.; Yan, J. Colorless polyimides derived from isomeric dicyclohexyl-tetracarboxylic dianhydrides for optoelectronic applications. *Polymer* **2018**, *134*, 8–19. [CrossRef]

44. Hasegawa, M.; Watanabe, Y.; Tsukuda, S.; Ishii, J. Solution-processable colorless polyimides with ultralow coefficients of thermal expansion for optoelectronic applications. *Polym. Int.* **2016**, *65*, 1063–1073. [CrossRef]
45. Hasegawa, M.; Ichikawa, K.; Takahashi, S.; Ishii, J. Solution-processable colorless polyimides derived from hydrogenated pyromellitic dianhydride: Strategies to reduce the coefficients of thermal expansion by maximizing the spontaneous chain orientation behavior during solution casting. *Polymers* **2022**, *14*, 1131. [CrossRef] [PubMed]
46. Yu, H.C.; Kumar, S.V.; Lee, J.H.; Oh, S.Y.; Chung, C.M. Preparation of robust, flexible, transparent films from partially aliphatic copolyimide. *Macromol. Res.* **2015**, *23*, 566–573. [CrossRef]
47. Tang, Y.; Li, L.; Ma, K.; Chen, G.; Wang, W.; Fang, X. Transparent and organosoluble cardo polyimides with different trans/cis ratios of 1,4-diaminocyclohexane via aromatic nucleophilic substitution polymerization. *Polym. Int.* **2018**, *67*, 598–605. [CrossRef]
48. Miao, J.; Hu, X.; Wang, X.; Meng, X.; Wang, Z.; Yan, J. Colorless polyimides derived from adamantane-containing diamine. *Polym. Chem.* **2021**, *11*, 6009–6016. [CrossRef]
49. Abdulhamid, M.A.; Ma, X.; Ghanem, B.S.; Pinnau, I. Synthesis and characterization of organo-soluble polyimides derived from alicyclic dianhydrides and a dihydroxyl-functionalized spirobisindane diamine. *ACS Appl. Polym. Mat.* **2019**, *1*, 63–69. [CrossRef]
50. Tapaswi, P.K.; Ha, C.S. Recent trends on transparent colorless polyimides with balanced thermal and optical properties: Design and synthesis. *Macromol. Chem. Phys.* **2019**, *220*, 1800313. [CrossRef]
51. Hasegawa, M.; Koyanaka, M. Polyimides containing *trans*-1,4-cyclohexane unit. Polymerizability of their precursors and low-CTE and low-K and High-T_g properties. *High Perform. Polym.* **2003**, *15*, 47–64. [CrossRef]
52. Hoshino, K.; Sato, H.; Ishii, J.; Hasegawa, M. Solution-processable colorless polyimides derived from novel cycloaliphatic tetracarboxylic dianhydride (3). *Polym. Prepr. Jpn.* **2019**, *68*, 1Pf090.
53. Kim, Y.S.; Jung, J.C. Synthesis and characterization of polyimides from 9,10-diphenyl-1,2,3,4,5,6,7,8-octahydro-2,3,6,7-anthracenetetracarboxylic 2,3:6,7-dianhydride. *Polym. Bull.* **2002**, *48*, 327–335. [CrossRef]
54. Kim, Y.S.; Jung, J.C. Synthesis and properties of polyimides derived from 9,10-dialkyloxy-1,2,3,4,5,6,7,8-octahydro-2,3,6,7-anthracenetetracarboxylic 2,3:6,7-dianhydrides. *J. Polym. Sci. Part A Polym. Chem.* **2002**, *40*, 1764–1774. [CrossRef]
55. Chi, J.H.; Shin, G.J.; Kim, Y.S.; Jung, J.C. Synthesis of new alicyclic polyimides by Diels-Alder polymerization. *J. Appl. Polym. Sci.* **2007**, *106*, 3823–3832. [CrossRef]
56. Briou, B.; Améduri, B.; Boutevin, B. Trends in the Diels–Alder reaction in polymer chemistry. *Chem. Soc. Rev.* **2021**, *50*, 11055–11097. [CrossRef]
57. Hasegawa, M.; Sensui, N.; Shindo, Y.; Yokota, R. Structure and properties of novel asymmetric biphenyl type polyimides. homo- and copolymers and blends. *Macromolecules* **1999**, *32*, 387–396. [CrossRef]
58. Hasegawa, M.; Matano, T.; Shindo, Y.; Sugimura, T. Spontaneous molecular orientation of polyimides induced by thermal imidization (2). In-plane orientation. *Macromolecules* **1996**, *29*, 7897–7909. [CrossRef]
59. Hasegawa, M.; Fujii, M.; Wada, Y. Approaches to improve the film ductility of colorless cycloaliphatic polyimides. *Polym. Adv. Technol.* **2018**, *29*, 921–933. [CrossRef]
60. Hasegawa, M.; Hoshino, Y.; Katsura, N.; Ishii, J. Superheat resistant polymers with low coefficients of thermal expansion. *Polymer* **2017**, *111*, 91–102. [CrossRef]
61. Baklagina, Y.G.; Milevskaya, I.S.; Efanova, N.V.; Sidorovich, A.V.; Zubkov, V.A. Structure of rigid-chain polyimides from pyromellitic dianhydride. *Vysokomol. Soedin.* **1976**, *A18*, 1235–1242.
62. Obata, Y.; Okuyama, K.; Kurihara, S.; Kitano, Y.; Jinda, T. X-ray Structure Analysis of an Aromatic Polyimide. *Macromolecules* **1995**, *28*, 1547–1551. [CrossRef]
63. Hasegawa, M.; Koseki, K. Poly(ester imide)s possessing low CTE and low water absorption. *High Perform. Polym.* **2006**, *18*, 697–717. [CrossRef]
64. Hasegawa, M.; Horii, S. Low-CTE polyimides derived from 2,3,6,7-naphthalenetetracarboxylic dianhydride. *Polym. J.* **2007**, *39*, 610–621. [CrossRef]
65. Hasegawa, M.; Takahashi, S.; Tsukuda, S.; Hirai, T.; Ishii, J.; Yamashina, Y.; Kawamura, Y. Symmetric and asymmetric spiro-type colorless poly(ester imide)s with low coefficients of thermal expansion, high glass transition temperatures, and excellent solution-processability. *Polymer* **2019**, *169*, 167–184. [CrossRef]
66. Hasegawa, M.; Kaneki, T.; Tsukui, M.; Okubo, N.; Ishii, J. High-temperature polymers overcoming the trade-off between excellent thermoplasticity and low thermal expansion properties. *Polymer* **2016**, *99*, 292–306. [CrossRef]
67. Takekoshi, T.; Wirth, J.G.; Heath, D.R.; Kochanowski, J.E.; Manello, J.S.; Webber, M.J. Polymer syntheses via aromatic nitro displacement reaction. *J. Polym. Sci. Part A Polym. Chem.* **1980**, *18*, 3069–3080. [CrossRef]